

RESEARCH ARTICLE

MR-based spatiotemporal anisotropic atrophy evaluation of hippocampus in Alzheimer's disease progression by multiscale skeletal representation

Na Gao¹  | Zhiyuan Liu² | Yuesheng Deng¹ | Hantao Chen¹ | Chenfei Ye^{3,4} | Qi Yang^{5,6,7} | Ting Ma^{1,3,4,8} 

¹Department of Electronic & Information Engineering, Harbin Institute of Technology (Shenzhen), Shenzhen, China

²Department of Computer Science, University of North Carolina at Chapel Hill, North Carolina, USA

³International Research Institute for Artificial Intelligence, Harbin Institute of Technology at Shenzhen, Shenzhen, China

⁴Peng Cheng Laboratory, Shenzhen, China

⁵Department of Radiology, Beijing Chaoyang Hospital, Capital Medical University, Beijing, China

⁶Key Lab of Medical Engineering for Cardiovascular Disease, Ministry of Education, Beijing, China

⁷Beijing Advanced Innovation Center for Big Data-Based Precision Medicine, Beijing, China

⁸Guangdong Provincial Key Laboratory of Aerospace Communication and Networking Technology, Harbin Institute of Technology (Shenzhen), Shenzhen, China

Correspondence

Ting Ma, Department of Electronics and Information, Harbin Institute of Technology at Shenzhen, Rm 1206, Information Building, HIT Campus, Shenzhen University Town, Nanshan District, Shenzhen, Guangdong Province, 518055, China.
Email: tma@hit.edu.cn

Funding information

Basic Research Foundation of Shenzhen Science and Technology Stable Support Program, Grant/Award Number: GXWD20201230155427003-20200822115709001; Innovation Team and Talents Cultivation Program of National Administration of Traditional Chinese Medicine, Grant/Award Number: ZYYCXTD-C-202004; National Natural Science Foundation of P.R. China, Grant/Award Numbers: 62276081, 62106113

Abstract

Increasing evidence has shown a higher sensitivity of Alzheimer's disease (AD) progression by local hippocampal atrophy rather than the whole volume. However, existing morphological methods based on subfield-volume or surface in imaging studies are not capable to describe the comprehensive process of hippocampal atrophy as sensitive as histological findings. To map histological distinctive measurements onto medical magnetic resonance (MR) images, we propose a multiscale skeletal representation (m-s-rep) to quantify focal hippocampal atrophy during AD progression in longitudinal cohorts from the Alzheimer's Disease Neuroimaging Initiative (ADNI). The m-s-rep captures large-to-small-scale hippocampal morphology by spoke interpolation over label projection on skeletal models. To enhance morphological correspondence within subjects, we align the longitudinal m-s-reps by surface-based transformations from baseline to subsequent timepoints. Cross-sectional and longitudinal measurements derived from m-s-rep are statistically analyzed to comprehensively evaluate the bilateral hippocampal atrophy. Our findings reveal that during the early AD progression, atrophy primarily affects the lateral-medial extent of the hippocampus, with a difference of 1.8 mm in lateral-medial width in 2 years preceding conversion ($p < .001$), and the medial head exhibits a maximum difference of 3.05%/year in local atrophy rate ($p = .011$) compared to controls. Moreover, progressive mild cognitive impairment (pMCI) exhibits more severe and widespread atrophy in the

This is an open access article under the terms of the [Creative Commons Attribution-NonCommercial-NoDerivs](https://creativecommons.org/licenses/by-nc-nd/4.0/) License, which permits use and distribution in any medium, provided the original work is properly cited, the use is non-commercial and no modifications or adaptations are made.

© 2023 The Authors. *Human Brain Mapping* published by Wiley Periodicals LLC.

head and body compared to stable mild cognitive impairment (sMCI), with a maximum difference of 1.21 mm in thickness in the medial head 1 year preceding conversion ($p = .012$). In summary, our proposed method can quantitatively measure the hippocampal morphological changes on 3T MR images, potentially assisting the pre-diagnosis and prognosis of AD.

KEYWORDS

Alzheimer's disease, hippocampal morphology, MRI, shape analysis, skeletal representations

1 | INTRODUCTION

Currently, the best-established structural imaging marker for early Alzheimer's disease (AD) diagnosis is the hippocampal atrophy (Dubois et al., 2014; Frisoni et al., 2010; Hill et al., 2014), which is mostly quantified as volume decrease in clinical studies. However, the overall hippocampal volume has low specificity discriminating potential mild cognitive impairment (MCI)-to-AD converters during AD prodromal stage (Lombardi et al., 2020; Ruchinkas et al., 2022; van Oostveen & de Lange, 2021). Evidence from AD pathology, histology, and ultra-high magnetic resonance imaging (MRI) imaging studies show that the AD pathology, the diffusion pattern of intra-neuronal neurofibrillary tangles (NFTs), causes selective neurodegeneration on hippocampal subfields (Braak & Braak, 1991, 1997b; Fukutani et al., 2000; Lace et al., 2009; Schönheit et al., 2004), and consequently leads to macroscopical complex atrophy on hippocampus. Increasing histological and 7T studies show sensitivity on the AD spectrum, supporting the hypothesis that the hippocampal atrophy is a continuous and dynamic process in AD continuum (McKiernan & O'Brien, 2017). One of the current major problems in AD interventions is to find early AD-affected local hippocampal atrophy patterns, so as to incorporate them into early structural biomarkers for AD pre-diagnosis and prognosis. The hippocampus is a primary site for the pathological hallmarks of AD, particularly the accumulation of NFT and the loss of neurons and neurites (de Flores et al., 2015). In AD preclinical stage, as one of the earliest targets of NFT, Cornu Ammonis (CA1) (specifically the CA1 stratum radiatum) is reported selectively thinning in most histological and 7T MRI studies (Braak & Braak, 1997a; Braak & Braak, 1997b; Kerchner et al., 2010; Scheff et al., 2007). Macrostructural studies that subdivide the hippocampus by larger scales show consistency that the atrophy on the anterior suffers more rapid atrophy than the posterior at AD preclinical stage (de Flores et al., 2015). However, to date, the relevant consistent local-specific findings have rarely been used as clinical imaging evidence to detect AD progression. Instead, the most widely used clinical method assessing the hippocampal atrophy, the medial temporal lobe atrophy (MTA) score, although provides more specific morphological information than volumetry, relies heavily on expertise (Kaushik et al., 2021). Currently, there is still a lack of a robust and reliable automated quantification method to comprehensively quantify the focal hippocampal atrophy based on clinical imaging, thus to narrow the gap between histological and clinical imaging findings.

The current hippocampal morphological representations based on structural MRI can be categorized into two main approaches: the subfield-volume-based (Gabere et al., 2020; Zeng et al., 2021; Zhang et al., 2020) and the surface-based representation (Biffi et al., 2020; Chapleau et al., 2020). The subfield-volume-based methods depend heavily on subfield segmentation accuracy, and do not provide sufficient descriptions of local atrophy. Therefore, many studies turn to the surface-based methods, which capture more subtle morphological variations than the volume-based methods. To discover more consistent disease-specific atrophy patterns on clinical imaging, the local atrophy of the macrostructure of the hippocampal shape, instead of the individual subfields, is investigated in these studies (Biffi et al., 2020; Chapleau et al., 2020; Gerardin et al., 2009; Shi et al., 2013; Tang et al., 2015). The main problem of the surface-based methods is that they indirectly describe the hippocampal atrophy by surface changes, whereas the "atrophy" is actually a morphological change on a three-dimensional (3D) anatomy. This problem leads to that the measurements derived from surface-based methods are inadequately interpretable in clinical settings and incomparable with histological findings. The relevant measurements are such as surface area contractions (Das et al., 2012; Tang et al., 2015), curvature changes (Shi et al., 2013), etc. Histologically, the process of the hippocampal atrophy is characterized by anisotropic decrease of local thickness, width and length on hippocampus (McKiernan & O'Brien, 2017), which can be hardly described by the surface-based representations. The 3D hippocampus is a thin bending archicortex with complex folds on its head (DeKraker et al., 2021). For such a single anatomical structure, the existed algorithms measuring thickness (Adler et al., 2018; Kharabian Masouleh et al., 2020) for 3D cortex cannot be directly transplanted into the hippocampus (Jones et al., 2000). It is also difficult to describe the hippocampal atrophy through radial atrophy thickness (Moon et al., 2018), because the thickness measuring lines may intersect with incorrect counterpart points due to the fold on head of hippocampus. These problems lead to inaccurate detection of local atrophy patterns. Furthermore, it is a challenge to detect subtle shape variations across AD development, compared with large inter-individual differences, since inaccurate morphological correspondence will lead to large variations across subjects. The commonly used registration-based methods are difficult to establish stable morphological correspondence between individuals with different number of folds (DeKraker et al., 2021). Overall, due to the complexity of the hippocampal structure and its atrophy, it is necessary to develop a

more comprehensive and precise representation to describe the hippocampal morphology.

To map histological distinctive features onto magnetic resonance (MR) images and identify unique local hippocampal atrophy patterns in early AD progression, we collect longitudinal MRI data from the Alzheimer's Disease Neuroimaging Initiative (ADNI) database, including amyloid- β positive progressive MCI (pMCI) patients, amyloid- β positive stable MCI (sMCI) patients and amyloid- β negative cognitive normal subjects (CN) with three scans for 1 year intermittent. To comprehensively describe the hippocampal morphological changes during the disease progression, we model the hippocampal shape by a multiscale skeletal representation (m-s-rep). The m-s-rep is developed based on skeletal representation (s-rep), which captures rich 3D intrinsic geometric properties of an object and is statistically stable (Liu et al., 2021; Pizer et al., 2020; Pizer et al., 2022; Tu et al., 2018). We develop the method by s-rep interpolation over surface labels projection, so as to assess the large-to-small scale hippocampal morphological variations during AD progression. Different from the surface-based methods, the measurements derived from our representation are more interpretable in clinical settings. To precisely characterize temporal properties of the atrophy patterns related to each experiment group, we improve the

intra-subject morphological correspondence by aligning the m-s-reps through a surface-based deformation field from the baseline hippocampus to the hippocampi at subsequent time points. We evaluate AD-sensitivity of the measurements derived from the m-s-reps by between-group hypothesis tests. The results show remarkable consistency between histological and 7T-MRI findings, and indicate distinctive hippocampal atrophy trajectories between the pMCI and sMCI patients.

2 | MATERIALS AND METHODS

We aim to evaluate local atrophy of the hippocampus related to the progression of pMCI and sMCI. For this purpose, we collect longitudinal data of A β -positive pMCI, sMCI and A β -negative cognitive normal controls from an open-source database. These data are preprocessed and then the hippocampi are represented by multiscale skeletal representations with a strategy to enhance longitudinal correspondence within subject. Cross-sectional and longitudinal measurements are extracted based on the m-s-reps. Finally, statistical analysis is performed on the extracted measurements. Figure 1 illustrates the entire pipeline of our method in this study.

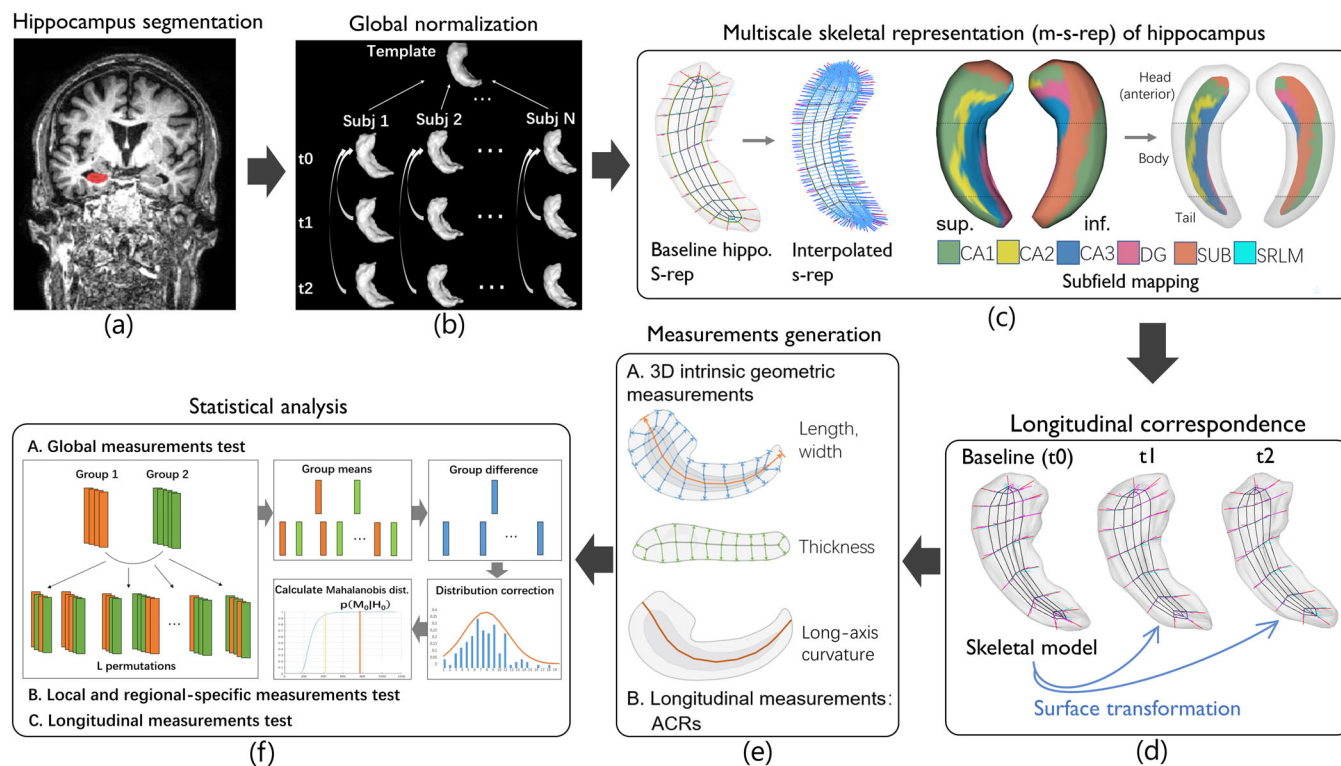


FIGURE 1 The modeling and analysis pipeline for the hippocampal atrophy evaluation. (a) The raw magnetic resonance imaging (MRI) T1-weighted images are segmented the hippocampi. (b) The longitudinal hippocampi are globally normalized. (c) The baseline hippocampi are represented by m-s-reps. (d) Longitudinal hippocampi are modeled by m-s-reps, with intra-subject correspondence improved by a deformation-based method. (e) The hippocampal atrophy can be characterized by both local and regional-specific spatiotemporal measurements. (f) The measurements are statistically tested sensitivity by between-group hypothesis test. The global shape measurement is tested using a permutation test framework tailored for s-rep data. ACR, annualized change rate; CA, cornu ammonis; DG, dentate gyrus; Sub, subiculum; SRLM: stratum radiatum and stratum lacunosum-moleculare; sup., superior; inf., inferior.

TABLE 1 Demographic information for the baseline data enrolled in this study.

	CN A β -	sMCI A β +	pMCI A β +
Number of subjects	81	88	67
Gender (male/female)	43/38	55/33	42/25
Age (years)	75.06 \pm 5.1	75.15 \pm 7.22	74.96 \pm 6.38
Education (years)	16.73 \pm 2.54	16.42 \pm 2.96	16.10 \pm 2.71
MMSE	29.12 \pm 1.11	28.32 \pm 1.77 *	27.31 \pm 1.89 *

Note: Group difference associated with gender was detected using chi-square test, group differences associated with age, education and neuropsychological scores were detected using non-parametric Kruskal–Wallis test. Data of age, education and MMSE are presented in mean \pm SD mode. Abbreviations: CN, cognitive normal; MMSE, Mini-Mental State Examination; pMCI+, amyloid- β positive progressive mild cognitive impairment; sMCI+, amyloid- β positive stable mild cognitive impairment.

* $p < .05$;

2.1 | Datasets

Data used in preparation of this study is obtained from the open-source Alzheimer's Disease Neuroimaging Initiative (ADNI) database (<http://adni.loni.usc.edu>) with three 3T MRI T1-weighted scans for 1 year intermittent. All participants have provided informed written consent before recruitment and filled out questionnaires approved by the respective Institutional Review Board (IRB). A subject is labeled as amyloid- β positive based on CSF A β 1-42 measurement (<192 pg/mL) (Landau et al., 2013; Shaw et al., 2009). Only the pMCI subjects who diagnosed as AD at their third visits and have positive status of CSF A β measurement at baseline are selected. The collected CN and sMCI subjects are age and gender matched with pMCI group. The selected sMCI subjects remain CSF A β positive and CN subjects remain A β negative through all the three visits. All enrolled sMCI and CN subjects keep the same diagnosis through all visits.

According to above criteria, a total of 236 subjects are involved in this study, including 81 CN controls, 88 sMCI, and 67 pMCI patients. The demographic information of their baseline examination is presented in Table 1.

2.2 | Data preprocessing

We deliver the hippocampal segmentation in a pipeline based on a 3D convolutional neural network. The method (called the HippMapp3r) has been proved outperformed some other approaches in AD and elderly population (Zeng et al., 2020). We test this method in longitudinal segmentation task, showing good performance in whole hippocampal volume and shapes. Each segmentation result is visually examined.

Global normalization is performed to rotationally align all the hippocampi and eliminate individual difference of global sizes. Because our aim is to evaluate the shape variations of hippocampus, no non-linear deformation is introduced into the preprocessing. The global normalization into common space is via an image registration strategy, illustrated in Figure 1b. First, all baseline hippocampi are linearly registered into a template hippocampus, which is calculated by averaging all baseline hippocampal shapes using the ANTs toolkit (Avants

et al., 2008). Second, each longitudinal hippocampus of a subject is registered into the baseline using a boundary-based linear registration of the flirt algorithm (Jenkinson et al., 2002) in FSL (Greve & Fischl, 2009).

The label images are extracted surface meshes and fitted with triangular meshes using SPHARM-PDM (Styner et al., 2006).

2.3 | Hippocampus modeling on longitudinal data

2.3.1 | The multiscale skeletal representation (m-s-rep) of the hippocampus

By considering the atrophy of the hippocampus as volume loss of a 3D anatomy, we initially represent the hippocampus based on the skeletal representation (s-rep). The s-rep provides a continuous interior-filling skeletal model of an object, which is formed by a set of spoke vectors (p, S) with tail at p and tip at $p + S$, where p represents the skeletal point that locate within the object and S represents the corresponding spoke vectors for p . The union of these spoke vectors forms the interior of the object, while the union of their tips forms the object's boundary. The tails of the spoke vectors, which form a folded double-sided surface, are called the skeletal locus. Mathematically, none of the spokes should intersect with each other. In this conventional view, each smooth point is associated with two spokes, called the up and down spokes (S_{up} and S_{down}), respectively. The spokes attached to fold points of the skeletal locus are called the crest spokes (S_{crest}). A typical hippocampus is fitted by the s-rep shown in the left panel of Figure 2. A detailed description of s-rep theory can be found in Pizer et al. (2020).

The initial s-reps of the hippocampi are generated using an automated method described in Liu et al. (2021). To balance the computational burden and representation accuracy, we select appropriate parameters for the s-rep models, which are described in detail in the Supplementary Material. From the s-rep data, we are able to represent the shape of the hippocampus by spokes. By continuously connecting the spoke tips, we get the implied surface of the hippocampus. As shown in Figure 2, a yellow area is filled with spokes and bounded by the implied surface. However, the implied surface of

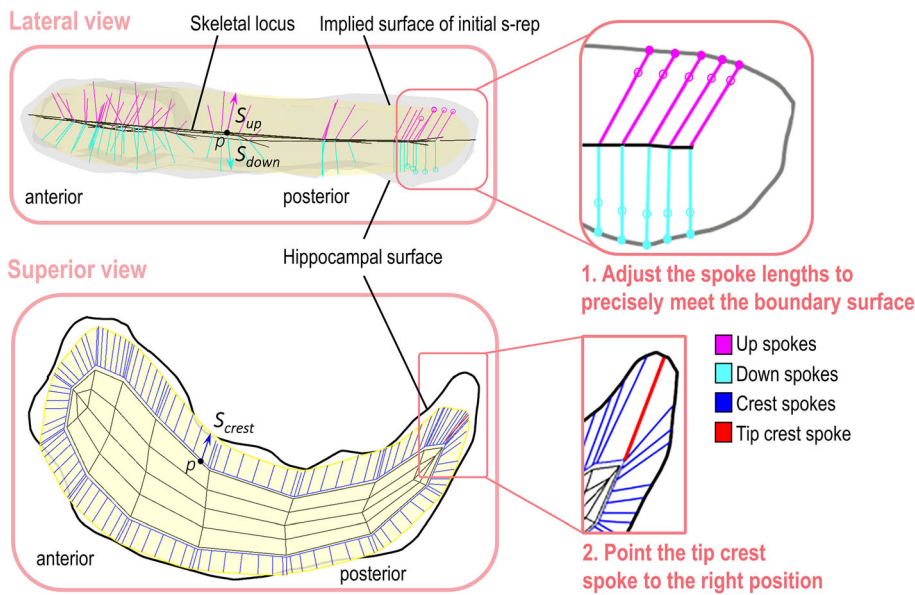


FIGURE 2 Original s-rep of a hippocampus and its improved s-rep. Left: lateral and superior view of a hippocampus and its initial s-rep (magenta, up spokes; cyan, down spokes; black, skeletal locus; yellow, implied surface). Right: improving the initial s-rep by: (1) adjusting the spoke lengths to precisely meet the boundary surface of the hippocampus (grey) and (2) pointing the tip crest spoke (red) to the right position.

the initial s-rep cannot precisely match the boundary surface of the hippocampus. Therefore, we adjust the lengths of the spokes to precisely meet the boundary surface of the hippocampus. In addition, the crest spoke attached on the tip of the skeleton locus may not always point to the tip of the hippocampus, which can result in incorrect locations for atrophy on hippocampal tails (an example is shown in the left panel of Figure 2). This incorrect location may lead to wrong measurement of length and long-axis curvature of the hippocampal shape. Therefore, we compulsorily position the tip crest spoke to the tip of the hippocampal tail. The tip of the hippocampal tail is defined as the point which has highest mean curvature on the surface of the hippocampal tail.

While the initial s-rep model can represent general shape of the hippocampus, it can neither capture subfields nor detailed local characterizations. To comprehensively evaluate the hippocampal atrophy during the disease progression, interpolation for original s-reps to cover all vertices on the hippocampal surface is implemented. Based on this interpolated s-rep, we propose a multiscale skeletal representation (m-s-rep). The term “multiscale” refers to the ability to represent the morphology of the hippocampus at different scales, allowing for the quantification of its morphological features from a global to a local level. The multiscale measurement method covers four scales that encompass (1) the global shape, (2) the tripartite partition (head, body, and tail), (3) the subfields within each partition, and (4) the detailed local thickness at each point on the surface.

A s-rep refinement method (Liu et al., 2021) is used to calculate the interpolated s-reps, which takes into account both surface fitness and s-rep geometry. A total of 1738 spokes are calculated to represent each individual hippocampus, with each vertex having a corresponding spoke in its neighborhood. In addition, the interpolated spokes are fitted to the original hippocampal surface to better characterize delicate local morphology. An example of the interpolated crest spokes of a hippocampus is shown in the right panel of Figure 1c. To realize regional analysis on the hippocampus, we project a

hippocampal subfield atlas onto the spokes of the hippocampus. Specifically, we use an averaged histological and 7T MRI-derived atlas (Adler et al., 2018) as a template and project the subfields on the surface onto each implied surface of the hippocampus by point-wise surface correspondence built by the SPHARM-PDM (spherical harmonic description point distribution models) (Styner et al., 2006). Then, each spoke tip is assigned to the subfield label according to its nearest point on the implied surface. Subfield labels on the boundary surface are mapped to the skeletal locus through spokes, as shown in Figure 1c. By projection from subfields to spokes, we can group the spokes by regions, and then generate regional measurements from these spokes.

2.3.2 | Improving correspondence on longitudinal data

The determination of point-wise correspondence across objects is a key subject in morphological analysis. The s-rep model offers intrinsic geometric characteristics that facilitate the establishment of cross-sectional correspondence by utilizing transformations from ellipses (Liu et al., 2021). However, the cross-sectional correspondence is insufficient for intra-subject analysis. Our basic assumptions are that the anatomical surfaces of the hippocampi remain smooth over time, and individual hippocampi undergo relatively small variations. This is typically observed in the prodromal stage of AD, where the hippocampi experience minor variations. To enhance longitudinal correspondence, we propose a strategy that involves deforming the baseline s-rep to align with the observed hippocampi at different time points. First, we establish surface correspondence among intra-individuals using the SPHARM-PDM method. We place dense control points on each vertex of the baseline surface mesh, and employ the thin-plate spline (TPS) method to smoothly transform the surface and its m-s-rep to fit the hippocampal surfaces observed at other time

points. The deformed m-s-reps are then refined to better fit the surface boundaries while preserving the s-rep geometry. This process is illustrated in Figure 1d.

2.3.3 | Measurement of the hippocampal morphology

We represent the global shape of a hippocampus by its s-rep, which consists of spoke locations, directions and lengths. Although features derived directly from m-s-reps are intrinsic geometric features for hippocampal morphology, they may not be easily interpretable in clinical settings. To enhance interpretability, we introduce new measurements based on the m-s-rep. In particular, we quantify the hippocampal morphology by measuring its length (anterior–posterior extent), lateral-medial width (lateral-medial extent), thickness (superior–inferior extent), and curvature of the long-axis (anterior–posterior axis). To obtain regional-specific thickness and width, we compute the average measurements for each region. Detailed definitions for these measurements are provided below.

The hippocampal long-axis can be represented by the central line of the skeletal locus and two crest spokes attached at the end of the long axis. We define the length of the whole hippocampus as the length of the long-axis. A length measuring line is shown in orange in the top panel of Figure 1e. Similarly, we define the lateral-medial width of the hippocampus by measuring the distance between the lateral and medial edges of the skeletal sheet, while adding the lengths of the corresponding two crest spokes located at the tips of the width measuring lines. The blue lines in the top panel of Figure 1e illustrate this measurement.

The thickness of the hippocampus, measured in the superior–inferior direction, is determined by summing the lengths of the up and down spokes, as illustrated in the middle panel of Figure 1e. This definition of thickness is robust in measuring the thickness at folds and guarantees that each point on the surface has a unique thickness value. In addition, this definition can be seen as a reasonable simplification of the thickness defined by Laplace's equation, as previously described by (Jones et al., 2000; Tustison et al., 2014).

To calculate the thickness and lateral-medial width of the subfield/tripartition of the hippocampus, we group the spokes by labels and compute the means of measurements from spokes belong to the same labels. The thickness between the superior and inferior surfaces involves two subfield labels. We represent the regional thickness as “the subfield label on the superior surface + the subfield label on the inferior surface,” for example, “CA1 + SUB.”

The long-axis curvature is determined by curvature of a discrete curve on the skeletal locus surface (Renka, 2005). The bottom panel of Figure 1e shows an example of long-axis of the hippocampus based on m-s-rep. The bending (curvature increase) or straightening (curvature decrease) of the long-axis is a consequence of non-uniform atrophy of the medial-lateral or superior–inferior hippocampus. Considering that previous research has identified the long-axis curvature as a significant different feature between individuals with AD and

normal controls (Adler et al., 2018), we believe that it has potential to be a valuable measurement for quantifying hippocampal atrophy.

2.3.4 | Longitudinal measurements for hippocampal atrophy

To evaluate temporal variations, we define longitudinal measurements by the annualized change rate (ACR) of above cross-sectional measurements (thickness, lateral-medial width, and long-axis curvature). The ACR of each cross-sectional measurement is defined as the slope of linear regression of all longitudinal mean measurements vs. scan date differences from baseline (Xie et al., 2020). Note that to correct for individual differences in head size, we divide the absolute hippocampal volume by the intracranial volume.

2.4 | Statistical analysis

We analysis the global shape measurement using a specific strategy. It is important to note that the spoke lengths are represented as real numbers in the Euclidean space, while the spoke positions and directions are defined in the three-dimensional spherical space. Therefore, the geometric elements of the spokes exist in the non-Euclidean space and exhibit spatial correlation (Pizer et al., 2020). This poses a critical challenge for statistically analyzing measurements derived from the skeletal model. To address these issues, we adopt a permutation test tailored for the s-rep features proposed by (Schulz et al., 2016) to test global shape difference between groups. To be specific, we first calculate means for a group of hippocampal s-reps by the composite principal nested sphere (CPNS) method (Pizer et al., 2020), which has been proved with superior performance in dealing with s-rep data. In CPNS, the abstract space of the s-rep data is separated into several spheres and real spaces. The real variables represent the lengths of the spokes and the sizes of the shapes, ensuring that they are all positive. These variables are log-transformed and rescaled to make them comparable with each other, and then the arithmetic means are calculated. The analysis of the spherical parts begins with the data on a high dimensional sphere, then iteratively fit a lower dimensional subspheres by an analytical computation of means (Pizer et al., 2013). The group means difference concerning both Euclidean and non-Euclidean components is constructed (the difference between spoke directions are measured by longitude and latitude differences). To account for the multivariate nature of the s-rep elements, these differences are mapped to a standard normal distribution, and the covariance matrix is estimated. Next, based on the cutoff value for the empirical distribution of the Mahalanobis distance, a global test is performed to identify global shape differences between groups. Individual features tests are conducted based on a single multivariate test with appropriate FWER inferences. Details of the method can be found in (Schulz et al., 2016). The statistical analysis code by CPNS non-Euclidean hypothesis test is uploaded on calliegao/m-s-rep (github.com).

We test the volume, regional and local scale measurements, including volume, length, thickness, lateral-medial width, long-axis curvature, local thickness, and longitudinal measurements using general linear models. Each measurement is set as the dependent variable, group membership as the factor of interest, age as covariate. Sex is included as an additional covariate for cross-sectional volume measurements. FDR correction for multiple comparisons is performed (Benjamini & Yekutieli, 2001). Cohen's d is used to measure the effect size (d), which can be considered as small (0.2), medium (0.5), or large (0.8).

3 | RESULTS

The statistical analysis results for group comparisons are summarized in Table 2 and Figures 3–6. The descriptions of the results are in details below.

3.1 | Difference between the pMCI progression and aging on cross-sectional measurements

3.1.1 | Left hippocampus

As shown in Table 2, we find significant global shape difference between the pMCI and CN group, and an increase of test statistics from t_0 to t_2 . As shown in Figure 3aA, the left hippocampus of pMCI group has significantly less volume than the CN controls at all-time points ($p_{t_0} < 0.001$, $d_{t_0} = 1.30$; $p_{t_1} < 0.001$, $d_{t_1} = 1.38$; $p_{t_2} < 0.001$, $d_{t_2} = 1.43$).

When tripartite the hippocampus into head, body, and tail, as shown in Figure 3aA,b, we observe that the pMCI group has significant less lateral-medial width in head ($p_0 < 0.001$, $d_{t_0} = 0.89$; $p_{t_1} < 0.001$, $d_{t_1} = 0.91$; $p_{t_2} < 0.001$, $d_{t_2} = 1.01$), body ($p_{t_0} < 0.001$, $d_{t_0} = 0.89$;

$p_{t_1} < 0.001$, $d_{t_1} = 0.98$; $p_{t_2} < 0.001$, $d_{t_2} = 1.00$) and tail ($p_{t_0} < 0.001$, $d_{t_0} = 0.85$; $p_{t_1} < 0.001$, $d_{t_1} = 0.88$; $p_{t_2} < 0.001$, $d_{t_2} = 0.96$) than the CN controls at all time points. As is shown in Figure 3aC, in 2 years preceding conversion, the means of width for the pMCI group (head: 17.17 ± 1.80 mm, body: 14.24 ± 1.67 mm, tail: 15.40 ± 1.94 mm) has around 1.8 mm less than those of the CN group (head: 18.96 ± 1.83 mm, body: 15.95 ± 1.75 mm, tail: 17.24 ± 1.97 mm).

We further investigate differences in the subfield-relevant regional thickness. The measurements that have significant group difference between the pMCI and CN groups through all time points include thickness in CA1 + SUB ($p_{t_0} = 0.045$, $d_{t_0} = 0.36$; $p_{t_1} = 0.002$, $d_{t_1} = 0.53$; $p_{t_2} < 0.001$, $d_{t_2} = 0.61$) and CA1 + CA1 in the head ($p_{t_0} < 0.001$, $d_{t_0} = 0.64$; $p_{t_1} < 0.001$, $d_{t_1} = 0.69$; $p_{t_2} < 0.001$, $d_{t_2} = 0.73$), CA1 + CA1 in the body ($p_{t_0} < 0.001$, $d_{t_0} = 0.89$; $p_{t_1} < 0.001$, $d_{t_1} = 1.00$; $p_{t_2} < 0.001$, $d_{t_2} = 0.97$) and DG + SUB ($p_{t_0} = 0.038$, $d_{t_0} = 0.42$; $p_{t_1} = 0.002$, $d_{t_1} = 0.58$; $p_{t_2} = 0.002$, $d_{t_2} = 0.53$) in the tail.

The first row of Figure 4a presents results for local thickness comparisons for the pMCI and CN groups at each time point. The largest effect size is 1.17 in the lateral part of the body (CA1 + CA1 region), where the difference is 1.17 mm ($p < .001$, $M_{pMCI} = 10.69$ mm, $SD_{pMCI} = 2.00$ mm; $M_{CN} = 11.86$ mm, $SD_{CN} = 2.12$ mm).

3.1.2 | Right hippocampus

As shown in Table 2, we find significant global shape differences between the pMCI and CN group. In Figure 5aA, the right hippocampus of the pMCI group has significantly less volume than the CN controls at all-time points ($p_{t_0} < 0.001$, $d_{t_0} = 1.36$; $p_{t_1} < 0.001$, $d_{t_1} = 1.41$; $p_{t_2} < 0.001$, $d_{t_2} = 1.48$).

Regarding the measurements in hippocampal head, body, and tail, we shown in Figure 5aA that the pMCI group has significant less lateral-medial width in head ($p_{t_0} < 0.001$, $d_{t_0} = 0.91$; $p_{t_1} < 0.001$, $d_{t_1} = 0.96$; $p_{t_2} < 0.001$, $d_{t_2} = 1.00$), body ($p_{t_0} < 0.001$, $d_{t_0} = 0.98$;

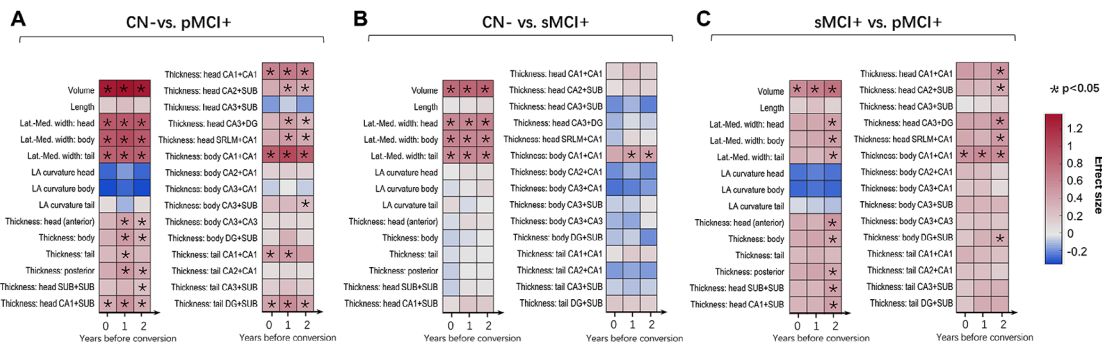
TABLE 2 Global shape hypothesis test results using the non-Euclidean hypothesis test.

Experiment groups	Left/right hippocampus		t0	t1	t2
CN vs. pMCI	Left	<i>p</i> -Values	0	0	0
		Statistics*	4948.910	5232.854	5560.110
	Right	<i>p</i> -Values	0	0	0
		Statistics*	5642.559	5573.506	5610.743
CN vs. sMCI	Left	<i>p</i> -Values	.010	.006	.002
		Statistics*	2273.496	2376.276	3208.199
	Right	<i>p</i> -Values	0	0	.0002
		Statistics*	4368.167	5720.886	3157.594
sMCI vs. pMCI	Left	<i>p</i> -Values	.1860	.0428	.0326
		Statistics*	528.202	1230.866	1103.784
	Right	<i>p</i> -Values	.002	.0001	0
		Statistics*	2217.153	3717.612	5122.539

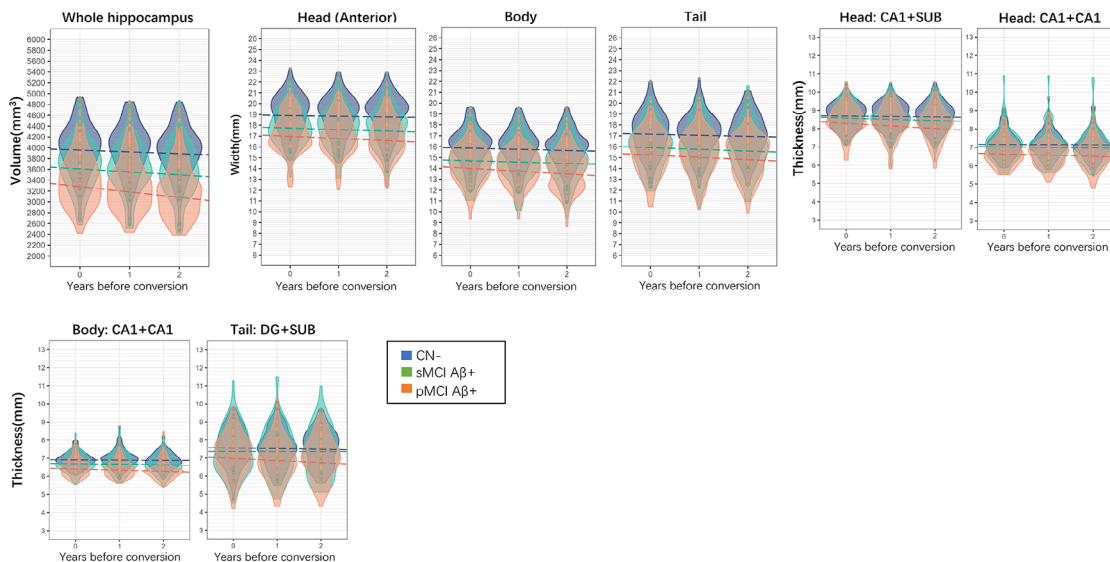
Note: *The Mahalanobis distances.

Abbreviations: CN, cognitive normal; pMCI, progressive mild cognitive impairment; sMCI, stable mild cognitive impairment.

(a) Group comparisons in cross-sectional measurements (global and regional measurements: volume, length, LA curvature, width and thickness on each time point)



(b) Distributions and trajectories of measurements across time (only show cross-sectional measurements with significant group differences at all time points)



(c) Group comparisons in longitudinal measurements (Annualized atrophy rate(%/year) of global and regional measurements)

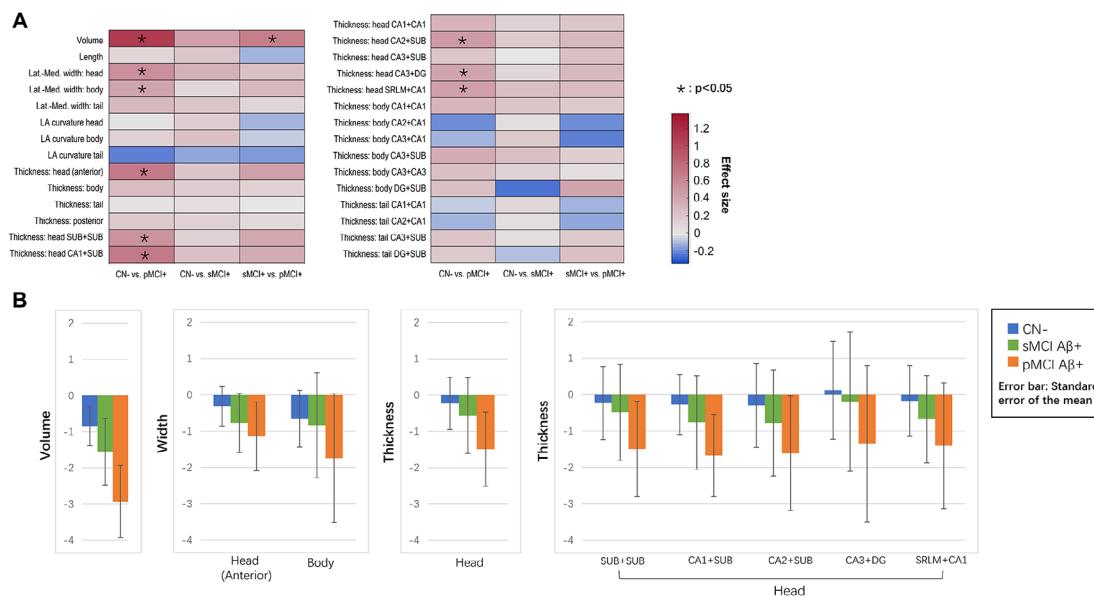
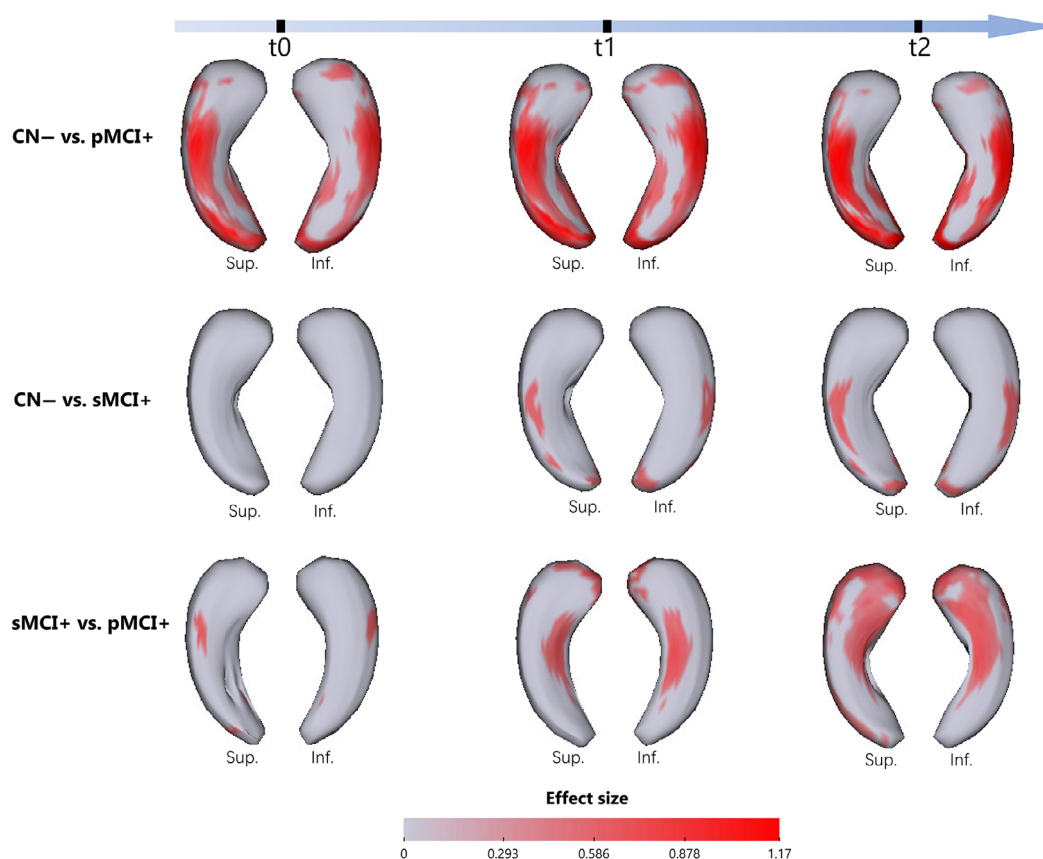


FIGURE 3 Legend on next page.

(a) Cross-sectional local thickness



(b) Longitudinal thickness decreasing rate

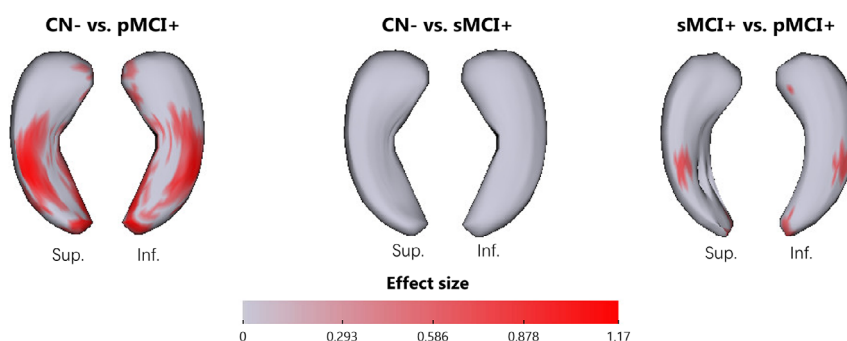
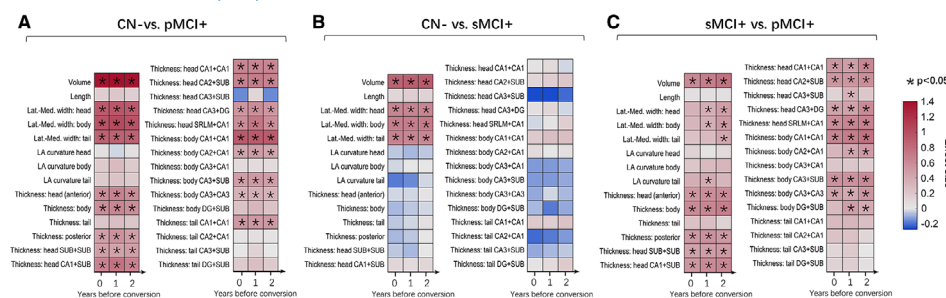


FIGURE 4 Left hippocampus: statistical analysis results of local thickness during the last 2 years of pMCI-to-AD conversion. (a) Between-group comparisons results on local thickness at each time point (t0, t1, t2). The color bar shows effect size using Cohen's d (CN - pMCI, CN - sMCI, sMCI - pMCI) at each time point. (b) Between-group comparisons results for annualized thickness-decreasing rate. The color bar shows effect size using Cohen's d (CN - pMCI, CN - sMCI, sMCI - pMCI). CN-, amyloid- β negative cognitive normal; pMCI+, amyloid- β positive progressive mild cognitive impairment; sMCI+, amyloid- β positive stable mild cognitive impairment; sup., superior; inf., inferior.

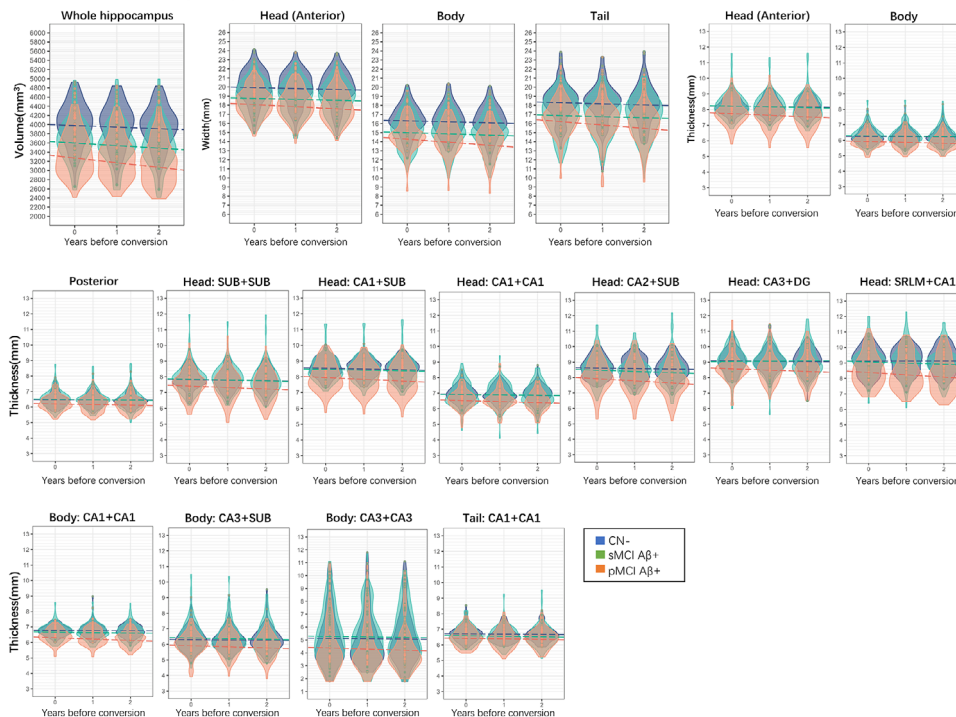
FIGURE 3 Left hippocampus: statistical analysis results of global and regional hippocampal atrophy during the last 2 years of pMCI-to-AD conversion. (a) (A, B, C) Between-group comparisons results on cross-sectional measurements. The effect size using Cohen's d is shown as color bar (CN - pMCI, CN - sMCI, sMCI - pMCI), and the p value $<.05$ is marked by star. (b) Distributions by violin plots, and trajectories of the measurements by line graphs using linear regression to see the changes of each group over time. Because we focus on features sensitive to diseases at early stage of disease and change over time, only the measurements show significant group difference at all time points are depicted. Note that the negative values in regional long-axis curvatures suggest that one group of hippocampi are more curved than the other group along the anterior-posterior dimension of the hippocampus. (c) (1) Between-group comparisons results on longitudinal measurements. The effect size using Cohen's d is shown as color bar (CN - pMCI, CN - sMCI, sMCI - pMCI), and the p value $<.05$ is marked by star. (2) Means and standard errors of longitudinal measurements for each group. CN-, amyloid- β negative cognitive normal; LA curvature, long-axis curvature; Lat., lateral; Med., medial; pMCI+, amyloid- β positive progressive mild cognitive impairment; sMCI+, amyloid- β positive stable mild cognitive impairment.

FIGURE 5 Right hippocampus: statistical analysis results of global and regional hippocampal atrophy during the last 2 years of pMCI-to-AD conversion. (a) (A, B, C) Between-group comparisons results on cross-sectional measurements. The effect size using Cohen's *d* is shown as color bar (CN – pMCI, CN – sMCI, sMCI – pMCI), and the *p* value <.05 is marked by star. (b) Distributions by violin plots, and trajectories of the measurements by line graphs using linear regression to see the changes of each group over time. Because we focus on features sensitive to diseases at early stage of disease and change over time, only the measurements show significant group difference at all time points are depicted. Note that the negative values in regional long-axis curvatures suggest that one group of hippocampi are more curved than the other group along the anterior–posterior dimension of the hippocampus. (c) (1) Between-group comparisons results on longitudinal measurements. The effect size using Cohen's *d* is shown as color bar (CN – pMCI, CN – sMCI, sMCI – pMCI), and the *p* value <.05 is marked by star. (2) Means and standard errors of longitudinal measurements for each group. CN–, Amyloid- β negative cognitive normal; LA curvature, long-axis curvature; Lat., lateral; Med., medial; pMCI+, amyloid- β positive progressive mild cognitive impairment; sMCI+, amyloid- β positive stable mild cognitive impairment.

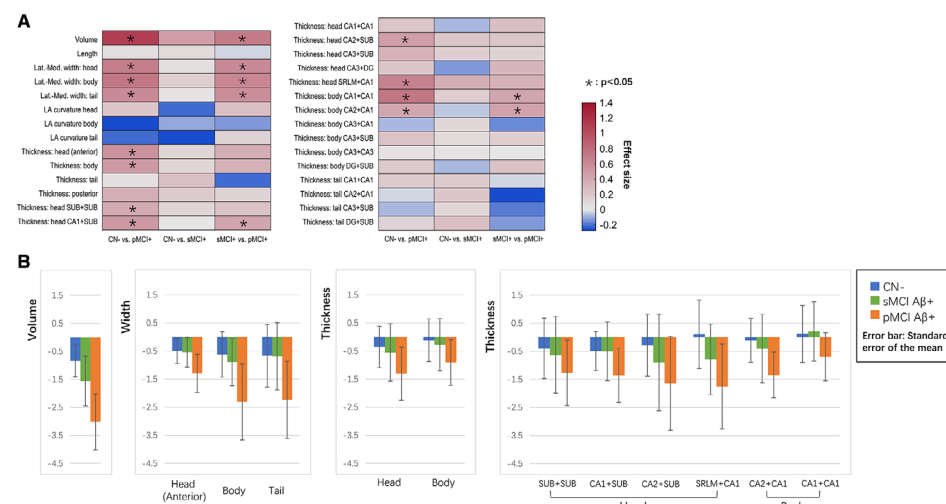
(a) Group comparisons in cross-sectional measurements (global and regional measurements: volume, length, LA curvature, width and thickness on each time point)



(b) Distributions and trajectories of measurements across time (only show cross-sectional measurements with significant group differences at all time points)



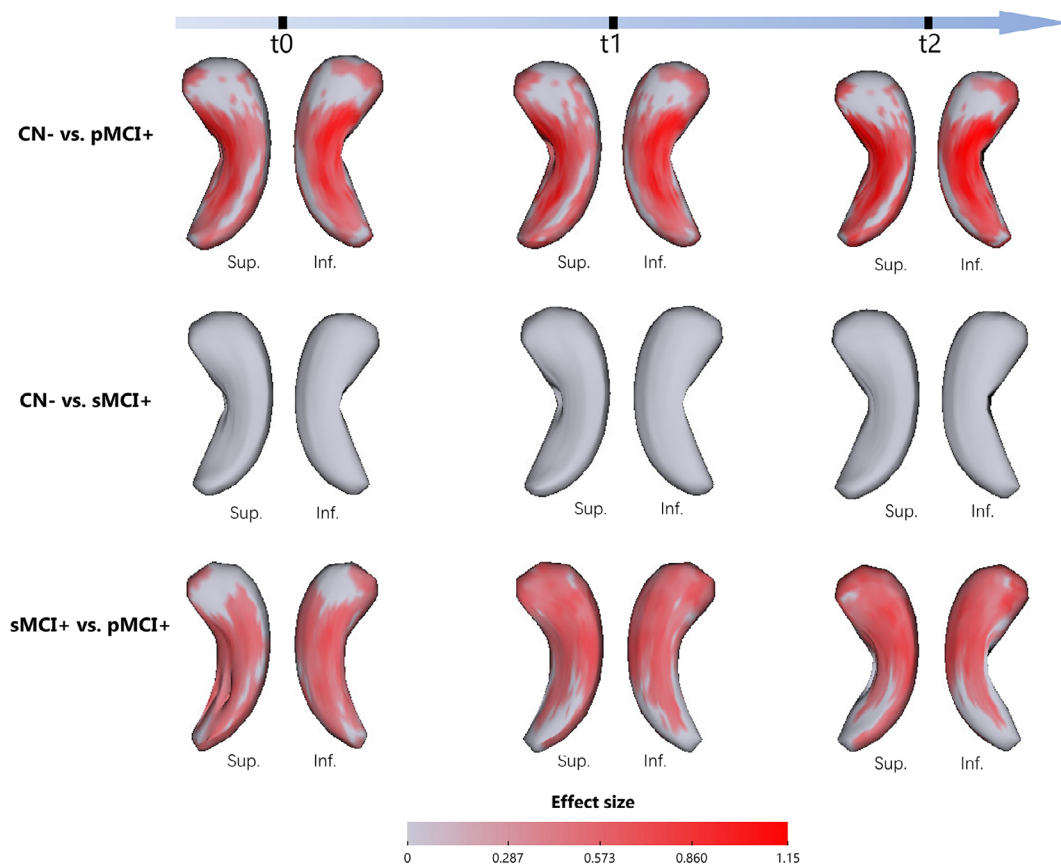
(c) Group comparisons in longitudinal measurements (Annualized atrophy rate(%/year) of global and regional measurements)



$p_{t1} < 0.001$, $d_{t1} = 1.02$; $p_{t2} < 0.001$, $d_{t2} = 1.11$) and tail ($p_{t0} < 0.001$, $d_{t0} = 0.87$; $p_{t1} < 0.001$, $d_{t1} = 0.87$; $p_{t2} < 0.001$, $d_{t2} = 0.99$) than the CN controls at all-time points. From Figure 3aC, we observe that

the means of lateral-medial width for the pMCI group (head: 18.29 ± 1.54 mm, body: 14.57 ± 1.64 mm, tail: 16.55 ± 1.92 mm) has around 1.8 mm less than those of the CN group (head: 20.03 ± 1.82 mm,

(a) Cross-sectional local thickness



(b) Longitudinal thickness decreasing rate

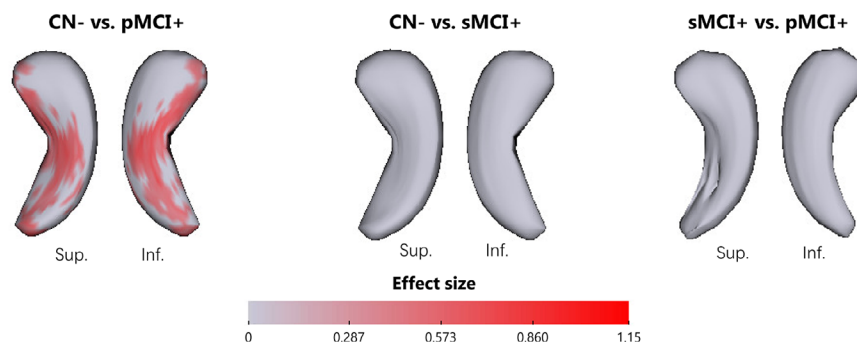


FIGURE 6 Right hippocampus: statistical analysis results of local thickness during the last 2 years of pMCI-to-AD conversion. (a) Between-group comparisons results on local thickness at each time point (t_0 , t_1 , t_2). The color bar shows effect size using Cohen's d (CN - pMCI, CN - sMCI, sMCI - pMCI) at each time point. (b) Between-group comparisons results for annualized thickness-decreasing rate. The color bar shows effect size using Cohen's d (CN - pMCI, CN - sMCI, sMCI - pMCI). CN-, amyloid- β negative cognitive normal; pMCI+, amyloid- β positive progressive mild cognitive impairment; sMCI+, amyloid- β positive stable mild cognitive impairment; sup., superior; inf., inferior.

body: 16.39 ± 1.61 mm, tail: 18.43 ± 1.99 mm) in 2 years before AD conversion. Moreover, the pMCI group has less thickness in head ($p_{t_0} < 0.001$, $d_{t_0} = 0.58$; $p_{t_1} < 0.001$, $d_{t_1} = 0.65$; $p_{t_2} < 0.001$, $d_{t_2} = 0.74$), body ($p_{t_0} < 0.001$, $d_{t_0} = 0.58$; $p_{t_1} < 0.001$, $d_{t_1} = 0.64$; $p_{t_2} < 0.001$, $d_{t_2} = 0.74$) and posterior ($p_{t_0} = 0.004$, $d_{t_0} = 0.55$; $p_{t_1} = 0.002$, $d_{t_1} = 0.48$; $p_{t_2} < 0.001$, $d_{t_2} = 0.60$) than the CN group.

As shown in Figure 5a,b, measurements of the pMCI group in regions of hippocampal head that are significant less than those of the

CN group includes thickness in SUB + SUB ($p_{t_0} = 0.003$, $d_{t_0} = 0.47$; $p_{t_1} = 0.003$, $d_{t_1} = 0.46$; $p_{t_2} = 0.001$, $d_{t_2} = 0.58$), CA1 + SUB ($p_{t_0} = 0.045$, $d_{t_0} = 0.67$; $p_{t_1} = 0.002$, $d_{t_1} = 0.75$; $p_{t_2} < 0.001$, $d_{t_2} = 0.80$), CA1 + CA1 ($p_{t_0} < 0.001$, $d_{t_0} = 0.63$; $p_{t_1} < 0.001$, $d_{t_1} = 0.68$; $p_{t_2} < 0.001$, $d_{t_2} = 0.68$), CA2 + SUB ($p_{t_0} < 0.001$, $d_{t_0} = 0.66$; $p_{t_1} < 0.001$, $d_{t_1} = 0.69$; $p_{t_2} < 0.001$, $d_{t_2} = 0.68$), CA3 + DG ($p_{t_0} = 0.001$, $d_{t_0} = 0.53$; $p_{t_1} < 0.001$, $d_{t_1} = 0.59$; $p_{t_2} < 0.001$, $d_{t_2} = 0.66$) and SRLM+CA1 ($p_{t_0} < 0.001$, $d_{t_0} = 0.59$; $p_{t_1} < 0.001$,

$d_{t1} = 0.73$; $p_{t2} < 0.001$, $d_{t2} = 0.83$). Significant difference are also found in thickness of several regions in hippocampal body, including the CA1 + CA1 ($p_{t0} < 0.001$, $d_{t0} = 0.91$; $p_{t1} < 0.001$, $d_{t1} = 0.92$; $p_{t2} < 0.001$, $d_{t2} = 1.10$), CA2 + CA1 ($p_{t0} = 0.013$, $d_{t0} = 0.42$; $p_{t1} = 0.007$, $d_{t1} = 0.46$; $p_{t2} < 0.001$, $d_{t2} = 0.58$), CA3 + SUB ($p_{t0} = 0.005$, $d_{t0} = 0.49$; $p_{t1} = 0.004$, $d_{t1} = 0.50$; $p_{t2} < 0.001$, $d_{t2} = 0.59$) and CA3 + CA3 ($p_{t0} = 0.013$, $d_{t0} = 0.44$; $p_{t1} = 0.031$, $d_{t1} = 0.38$; $p_{t2} = 0.002$, $d_{t2} = 0.52$). Thickness in the CA1 + CA1 of the hippocampal tail of the pMCI group is less than that of the CN group ($p_{t0} = 0.002$, $d_{t0} = 0.49$; $p_{t1} = 0.002$, $d_{t1} = 0.50$; $p_{t2} < 0.001$, $d_{t2} = 0.55$). In 2 years preceding to AD conversion, the two groups have largest difference of 0.70 mm in CA3 + CA3 region in the body ($p_{t0} = 0.013$, $d = 0.44$; $M_{pMCI} = 4.45$ mm, $SD_{pMCI} = 1.99$ mm; $M_{CN} = 5.15$ mm, $SD_{CN} = 2.11$ mm).

The first row of Figure 6a presents results for local thickness comparisons of the pMCI and CN groups at each time point. Two years before conversion, the largest effect size is 1.15 in the CA3 + CA3 region in medial part of the body, where the difference is 1.47 mm ($M_{pMCI} = 12.20$ mm, $SD_{pMCI} = 2.15$ mm; $M_{CN} = 13.66$ mm, $SD_{CN} = 2.18$ mm).

3.2 | Difference between the sMCI progression and aging on cross-sectional measurements

3.2.1 | Left hippocampus

The sMCI group has significant global shape difference from the CN group and an increasing of test statistics, as shown in Table 2. Figure 3aB presents the group comparison results for other global and regional measurements at three-time points between sMCI and CN groups. The sMCI group has less hippocampal volume than the CN group at all-time points ($p_{t0} < 0.001$, $d_{t0} = 0.79$; $p_{t1} < 0.001$, $d_{t1} = 0.81$; $p_{t2} < 0.001$, $d_{t2} = 0.84$).

As shown in Figure 3aB,D, The sMCI group has significant less lateral-medial width in head ($p_{t0} < 0.001$, $d_{t0} = 0.61$; $p_{t1} < 0.001$, $d_{t1} = 0.59$; $p_{t2} < 0.001$, $d_{t2} = 0.66$), body ($p_{t0} < 0.001$, $d_{t0} = 0.62$; $p_{t1} < 0.001$, $d_{t1} = 0.61$; $p_{t2} < 0.001$, $d_{t2} = 0.61$) and tail ($p_{t0} = 0.001$, $d_{t0} = 0.57$; $p_{t1} < 0.001$, $d_{t1} = 0.61$; $p_{t2} < 0.001$, $d_{t2} = 0.61$) than the CN controls at all-time points.

The second row of Figure 4a presents results for local thickness comparisons of the sMCI and CN groups at each time point. No local measurement has significant difference at all three-time points. The lateral of body and the tail tip show significant difference at the second time point.

3.2.2 | Right hippocampus

As shown in Table 2, the sMCI and CN groups have significant global shape difference. Figure 5aB presents that the right hippocampi of sMCI group have less volume than that of the CN group at all-time points ($p_{t0} < 0.001$, $d_{t0} = 0.88$; $p_{t1} < 0.001$, $d_{t1} = 0.88$; $p_{t2} < 0.001$, $d_{t2} = 0.92$).

As shown in Figure 5aA,b, the sMCI group has significant less lateral-medial width of head ($p_{t0} < 0.001$, $d_{t0} = 0.63$; $p_{t1} < 0.001$, $d_{t1} = 0.63$; $p_{t2} < 0.001$, $d_{t2} = 0.63$), body ($p_{t0} < 0.001$, $d_{t0} = 0.70$; $p_{t1} < 0.001$, $d_{t1} = 0.70$; $p_{t2} < 0.001$, $d_{t2} = 0.71$) and tail ($p_{t0} < 0.001$, $d_{t0} = 0.66$; $p_{t1} < 0.001$, $d_{t1} = 0.64$; $p_{t2} < 0.001$, $d_{t2} = 0.63$) than the CN controls at all-time points.

3.3 | Difference between the pMCI and sMCI progression on cross-sectional measurements

3.3.1 | Left hippocampus

The pMCI group has significant difference in global shape measurement compared with the sMCI group at the last two time points. Figure 3aC shows that the two groups have already shown significant difference in volume 2 years prior to conversion ($p_{t0} < 0.001$, $d_{t0} = 0.58$; $p_{t1} < 0.001$, $d_{t1} = 0.67$; $p_{t2} < 0.001$, $d_{t2} = 0.73$).

Among regional measurements, only the thickness of CA1 + CA1 in the body has significant group difference between the pMCI ($M_{t0} = 6.47$ mm, $SD_{t0} = 0.47$ mm) and sMCI group ($M_{t0} = 6.72$ mm, $SD_{t0} = 0.49$ mm) through all time points ($p_{t0} = 0.017$, $d_{t0} = 0.52$; $p_{t1} = 0.004$, $d_{t1} = 0.57$; $p_{t2} = 0.002$, $d_{t2} = 0.58$).

The third row of Figure 4a presents results for local thickness comparisons between the sMCI and pMCI groups at each time point. Although we observe significant differences in locations 2 years before AD conversion (mainly in the CA1 + CA1 region in the body), measurements at these locations do not show significant differences at subsequent time points. The medial part of body and the top of anterior show significant difference in the last year before AD conversion, where the largest difference is 1.21 mm ($p = .012$, $d = .595$, $M_{pMCI} = 10.31$ mm, $SD_{pMCI} = 1.67$ mm; $M_{sMCI} = 11.5$ mm, $SD_{sMCI} = 2.13$ mm) in SRLM+CA1.

3.3.2 | Right hippocampus

The pMCI group has significant difference in the global shape measurement compared with the sMCI group at all-time points. Figure 5aC shows that the right hippocampal volume of pMCI group is significant less than that of the CN group at all-time points ($p_{t0} < 0.001$, $d_{t0} = 0.60$; $p_{t1} < 0.001$, $d_{t1} = 0.67$; $p_{t2} < 0.001$, $d_{t2} = 0.76$).

The pMCI group has significant less thickness in head ($p_{t0} = 0.002$, $d_{t0} = 0.52$; $p_{t1} < 0.001$, $d_{t1} = 0.59$; $p_{t2} < 0.001$, $d_{t2} = 0.61$) and body ($p_{t0} = 0.001$, $d_{t0} = 0.59$; $p_{t1} < 0.001$, $d_{t1} = 0.64$; $p_{t2} < 0.001$, $d_{t2} = 0.68$) than the sMCI group. The pMCI group also has significant less thickness in the posterior ($p_{t0} = 0.003$, $d_{t0} = 0.50$; $p_{t1} = 0.002$, $d_{t1} = 0.54$; $p_{t2} = 0.003$, $d_{t2} = 0.51$) than that of the sMCI controls at all-time points.

Thickness in hippocampal head including SUB + SUB ($p_{t0} = 0.010$, $d_{t0} = 0.45$; $p_{t1} = 0.005$, $d_{t1} = 0.48$; $p_{t2} = 0.002$, $d_{t2} = 0.50$), CA1 + SUB ($p_{t0} = 0.002$, $d_{t0} = 0.53$; $p_{t1} < 0.001$, $d_{t1} = 0.61$; $p_{t2} < 0.001$, $d_{t2} = 0.64$), CA1 + CA1 ($p_{t0} = 0.003$, $d_{t0} = 0.52$; $p_{t1} = 0.005$,

$d_{t1} = 0.47$; $p_{t2} < 0.001$, $d_{t2} = 0.62$), CA2 + SUB ($p_{t0} = 0.002$, $d_{t0} = 0.52$; $p_{t1} = 0.001$, $d_{t1} = 0.54$; $p_{t2} < 0.001$, $d_{t2} = 0.59$), CA3+DG ($p_{t0} = 0.010$, $d_{t0} = 0.44$; $p_{t1} = 0.007$, $d_{t1} = 0.45$; $p_{t2} < 0.001$, $d_{t2} = 0.62$), SRLM + CA1 ($p_{t0} = 0.002$, $d_{t0} = 0.57$; $p_{t1} < 0.001$, $d_{t1} = 0.64$; $p_{t2} < 0.001$, $d_{t2} = 0.67$) of the pMCI group are less than those of the CN group. Thickness of regions in hippocampal body, including the CA1+CA1 ($p_{t0} < 0.001$, $d_{t0} = 0.64$; $p_{t1} < 0.001$, $d_{t1} = 0.70$; $p_{t2} < 0.001$, $d_{t2} = 0.78$), CA3+SUB ($p_{t0} = 0.002$, $d_{t0} = 0.54$; $p_{t1} = 0.002$, $d_{t1} = 0.55$; $p_{t2} < 0.001$, $d_{t2} = 0.59$) and CA3 + CA3 ($p_{t0} = 0.013$, $d_{t0} = 0.44$; $p_{t1} = 0.031$, $d_{t1} = 0.38$; $p_{t2} = 0.002$, $d_{t2} = 0.52$) of the pMCI group, are less than those of the CN group.

The third row of Figure 6a presents results for local thickness comparisons between the sMCI and pMCI groups at each time point. We observe that the pMCI group has less thickness of the body and medial head than the sMCI group in 2 years before conversion. Atrophy locations spread to whole part of the head at following time points. In 2 years before conversion, the two groups have largest difference of local thickness 0.80 mm ($p = .004$, $d = 0.52$, $M_{pMCI} = 6.05$ mm, $SD_{pMCI} = 1.12$ mm; $M_{sMCI} = 6.85$ mm, $SD_{sMCI} = 1.59$ mm) in the medial of the body (CA3 + CA3).

3.4 | Between-group differences on longitudinal measurements

3.4.1 | Left hippocampus

As shown in Figure 3cA, the pMCI group has significant higher volume decreasing rate than CN and sMCI groups ($p_{CNvs.pMCI} < 0.001$, $d_{CNvs.pMCI} = 1.08$; $p_{sMCIvs.pMCI} < 0.001$, $d_{CNvs.pMCI} = 0.66$). The pMCI group has higher decreasing rate in lateral-medial width of head ($p < .007$, $d = .54$) and body ($p < .043$, $d = .41$), and thickness of head ($p < .001$, $d = .69$) than the CN group, with the highest decreasing rate of 1.74%/year in the body among all regional measurements (Figure 3cB). Regarding subfield-relevant regional thickness, regions in SUB + SUB ($p = .007$, $d = .53$) and CA1 + SUB ($p = .003$, $d = .68$), CA2 + SUB ($p = .020$, $d = .47$), CA3 + DG ($p = .045$, $d = .41$) and SRLM + CA1 ($p = .030$, $d = .44$) in the hippocampal head of the pMCI group has higher thickness-decreasing rate than the CN group.

Figure 4b shows group comparison results of local thickness-decreasing rate. We observe that the pMCI group has higher focal atrophy rate than the CN controls, particularly in the middle and lateral part of the hippocampus. The largest difference is 3.05%/year ($p = .011$, $d = .53$, $M_{pMCI} = -2.82\%/year$, $SD_{pMCI} = 6.45\%/year$; $M_{CN} = 0.23\%/year$, $SD_{CN} = 4.66\%/year$) in the medial hippocampal head near SRLM. The sMCI and CN group has no significant differences in local thickness-decreasing rate. As shown in the last column, significant higher focal atrophy rate of the pMCI than the sMCI has been discovered mainly in a small lateral part of the hippocampus (CA2 + CA1 region in the body), with the largest difference of 2.89%/year ($p = .034$, $d = .54$, $M_{pMCI} = -2.87\%/year$, $SD_{pMCI} = 6.04\%/year$; $M_{pMCI} = -0.02\%/year$, $SD_{pMCI} = 4.34\%/year$) found in medial hippocampal head near SRLM.

3.4.2 | Right hippocampus

As shown in Figure 5a, the pMCI group has significant higher volume decreasing rate than CN and sMCI groups ($p_{CNvs.pMCI} < 0.001$, $d_{CNvs.pMCI} = 1.11$; $p_{sMCIvs.pMCI} < 0.001$, $d_{CNvs.pMCI} = 0.71$). The pMCI group has higher decreasing rate in lateral-medial width of head ($p_{CNvs.pMCI} < 0.001$, $d_{CNvs.pMCI} = 0.68$; $p_{sMCIvs.pMCI} < 0.001$, $d_{CNvs.pMCI} = 0.60$), body ($p_{CNvs.pMCI} < 0.001$, $d_{CNvs.pMCI} = 0.73$; $p_{sMCIvs.pMCI} < 0.001$, $d_{CNvs.pMCI} = 0.62$) and tail ($p_{CNvs.pMCI} < 0.001$, $d_{CNvs.pMCI} = 0.61$; $p_{sMCIvs.pMCI} < 0.001$, $d_{CNvs.pMCI} = 0.58$) than the CN and sMCI groups, with the highest decreasing rate of 2.31%/year in the body among all regional measurements (Figure 5cB). The pMCI group has significant higher thickness-decreasing rate in head ($p = .002$, $d = .55$) and body ($p = .013$, $d = .49$) than the CN group. Regarding subfield-relevant regional thickness, the pMCI group has higher thickness-decreasing rate than the CN group in several regions in the head including SUB + SUB ($p = .032$, $d = .384$), CA1 + SUB ($p = .004$, $d = .513$), CA2 + SUB ($p = .011$, $d = .48$) and SRLM+CA1 ($p < .001$, $d = .65$). The pMCI group also has less thickness-decreasing rate in CA1 + CA1 ($p < .001$, $d = .73$) and CA2 + CA1 ($p = .032$, $d = .42$) regions in the body than the CN group. The pMCI group has significant less thickness compared with sMCI group in CA1 + SUB ($p = .040$, $d = .42$) in the head and CA1 + CA1 ($p = .037$, $d = .43$), CA2 + CA1 ($p = .030$, $d = .45$) regions in the body.

Figure 6b shows group comparison results of local thickness-decreasing rate. We observe that the pMCI group has higher focal atrophy rates than the CN controls in the middle and medial part of the hippocampus. Local thickness of pMCI group shows highest decreasing rate of $-2.96\%/year$ ($SD = 5.70\%/year$) in the medial hippocampal head near SRLM, and the corresponding thickness change rate of sMCI and CN group in the corresponding location are 0.40%/year ($SD = 7.79\%/year$) and $-0.87\%/year$ ($SD = 5.56\%/year$), respectively. In addition, the largest difference between the two groups is 2.64%/year ($p = .021$, $d = .47$, $M_{pMCI} = -2.38\%/year$, $SD_{pMCI} = 6.12\%/year$; $M_{CN} = 0.26\%/year$, $SD_{CN} = 4.79\%/year$) in the medial hippocampal head near SRLM. The sMCI has no significant differences in local thickness-decreasing rate compared with CN and pMCI groups.

4 | DISCUSSION

We propose a shape model to evaluate the comprehensive hippocampal atrophy during prodromal AD based on 3T T1-weighted images. This shape model enables a large-to-small scale description of the spatiotemporal morphological changes in the hippocampus. We implement the method on longitudinal cohorts collected from the ADNI database, including Amyloid- β positive pMCI and sMCI patients, as well as Amyloid- β negative cognitive normal subjects with 3 scans for 1 year intermittent to evaluate cross-sectional and longitudinal hippocampal atrophy during the MCI progression. The main findings include that: (1) Hippocampal atrophy during AD progression is dominated by lateral-medial width decrease, with approximately 1.8 mm less than

normal individuals in the 2 years preceding conversion. The largest difference in local thickness-decreasing rates (left: 3.05%/year; right: 2.64%/year) compared to normal ageing is observed in the medial head of hippocampi. (2) The differences between pMCI and sMCI extend from the body to the head of the hippocampus, indicating distinctive hippocampal atrophy trajectories between pMCI and sMCI. The lateral head of the left hippocampus (SRLM + CA1) experiences thickness decrease of 1.21 mm in compared to sMCI 1 year before conversion. The local thickness-decreasing rate shows the highest difference of 2.89%/year in the medial head of the left hippocampi between pMCI and sMCI.

4.1 | The evaluation of hippocampal atrophy in 3T in-vivo MRI obtains consistent findings with MRI and histology studies

In this study, the observed annualized hippocampal volume decreasing rates of normal aging are 0.85%/year and 0.84%/year for the left and right hippocampi, comparable with that reported in a systematic review in (Fraser et al., 2015) (1.12% for ≥ 70 years old healthy adults). We observe 2.93%/year and 3.02%/year volume decrease in left and right hippocampus for pMCI, 1.55%/year and 1.56%/year for sMCI. The results are comparable with those reported MCI volumetric atrophy rate, ranging from 1.55%/year to 3.2%/year in 12 studies (Chincarini et al., 2016; Das et al., 2012; Holland et al., 2012; Iglesias et al., 2016; Jack et al., 2000; Kulason et al., 2019; Ledig et al., 2018; Leung et al., 2010; Morra et al., 2009; Schuff et al., 2009; Tward et al., 2017; Wolz et al., 2010; Xie et al., 2020). The difference of the reported atrophy rate in literatures is possibly due to the hippocampal segmentation approaches and different MCI stages included in the experiments.

Our method introduces interpretable measurements for hippocampal morphology that can be compared to histology findings. In this study, we observe the anterior–posterior extent of the hippocampus (referred to as “length” in this study) to be 46.69 mm ($SD = 2.30$ mm), which is lower than the 50 mm reported in histological literature (Witter & Amaral, 2004), but falls within the range of autopsy results (31–51 mm) reported in Adler et al. (2018).

Numbers of studies recognize that the severer anterior atrophy than the posterior is a pattern of AD distinct from normal aging (Adler et al., 2018; Chauveau et al., 2021; Martin et al., 2010). Our experiment reveals that the difference in anterior thickness between pMCI and CN is more pronounced than that in the posterior region during the MCI-to-AD conversion. Specifically, the difference in the anterior region of the left hippocampus is 0.42 mm ($M_{pMCI} = 7.97$ mm, $SD_{pMCI} = 0.82$ mm; $M_{CN} = 8.39$ mm, $SD_{CN} = 0.65$ mm), while in the posterior region it is 0.21 mm ($M_{pMCI} = 6.24$ mm, $SD_{pMCI} = 0.52$ mm; $M_{CN} = 6.45$ mm, $SD_{CN} = 0.48$ mm). Similarly, the mean difference in the anterior region of the right hippocampus is 0.55 mm ($M_{pMCI} = 7.63$ mm, $SD_{pMCI} = 0.83$ mm; $M_{CN} = 8.18$ mm, $SD_{CN} = 0.55$ mm), and in the posterior region it is 0.30 mm ($M_{pMCI} = 6.17$, $SD_{pMCI} = 0.50$; $M_{CN} = 6.47$, $SD_{CN} = 0.46$). Moreover,

we test the longitudinal measurements for anterior and posterior differences. The pMCI have higher thickness-decreasing rate in anterior than the posterior hippocampus ($p_{left} = 0.017$, $d_{left} = 0.46$; $p_{right} = 0.020$, $d_{right} = 0.40$). Additionally, in the right hippocampus, the lateral-medial width of the posterior decreasing rate is higher than the anterior ($p = .009$, $d = .48$). The thicknesses of the anterior hippocampus are -1.49% /year ($SD = 2.03\%$ /year) and -1.31% /year ($SD = 1.90\%$ /year) for the left and right side respectively, and the width of the posterior of the right hippocampus decreases -2.28% /year ($SD = 2.47\%$ /year) in pMCI. In conclusion, our results shows that the thickness reduction of the anterior hippocampus in individuals with pMCI is more severe and occurs at a higher decreasing rate than the posterior, consistent with (Adler et al., 2018) and (de Flores et al., 2015), and there is also a rapid decrease in the lateral-medial width of the posterior part of the right hippocampus.

In our results (Figures 3aA and 5aA), we observe that pMCI shows an atrophy pattern primarily distributed in CA1 and SUB in early AD, suggesting a similar diffusing pattern from CA1 and SUB to CA2, CA3, and DG (Braak et al., 1993; Braak & Braak, 1991; Fukutani et al., 2000; Gunten et al., 2006; Kril et al., 2002; Lace et al., 2009; Padurariu et al., 2012). Furthermore, our experiment revealed that the medial part of the hippocampal head (SRLM + CA1) exhibited the fastest atrophy in both the left and right hippocampi, with an annual rate of $2.89 \pm 5.69\%$ for the left side and $2.96 \pm 5.70\%$ for the right side. This finding aligns with previous histological and 7 T MRI studies, which have consistently shown selective thinning of CA1-SRLM in early AD (Braak & Braak, 1997a; Braak & Braak, 1997b; Kerchner et al., 2010; Scheff et al., 2007).

4.2 | Potential morphometric measures to differentiate A β positive pMCI and sMCI in prodromal AD

We observe a significant decrease in hippocampal volume in pMCI compared to age-matched sMCI. The volume decreasing rates in the pMCI group (Left: $2.93 \pm 2.14\%$ /year; Right: $3.02 \pm 2.09\%$ /year) are significantly higher than the sMCI (Left: $1.55 \pm 1.85\%$ /year; Right: $1.56 \pm 1.76\%$ /year) 2 years prior to AD conversion. In addition, we have also discovered other measurements that are comparable to volume in terms of p -values and effect size in the pMCI and sMCI comparison. The global shape of the hippocampus was also found to be a reliable indicator of group differences. Specifically, we observe a significant difference in the right hippocampus 2 years before AD conversion, with the difference increasing over time. Our analysis of regional and local measurements revealed that the pMCI exhibits more severe atrophy on bilateral hippocampi than sMCI. Specifically, various cross-sectional measurements show significant differences in the pMCI group, but not in the sMCI group, when compared to normal controls 2 years prior to AD conversion. Interestingly, the hippocampi of individuals with sMCI only exhibited a significant difference in the lateral-medial width compared to CN 2 years prior to AD conversion. In the early stages of Alzheimer's disease (AD), significant differences

have been observed between individuals with pMCI and sMCI even before conversion, with the differences spreading from the body to the head of the hippocampus. In the 2 years preceding conversion, the right hippocampus exhibits more severe and widespread atrophy, affecting the thickness of certain regions in the head and body, including CA1, SUB, and CA3 (Figures 3aC and 5aC). The differences in regional and local thickness between the two groups are found to be less than 1 mm in the 2 years prior to conversion (Figure 3b, Figure 5b), which is within the limits of the image resolution. The largest difference in local thickness, approximately 0.8 mm, is observed in the CA3 + CA3 region of the right hippocampal body. The largest difference of 1.21 mm is found in the lateral head of the left hippocampus (SRLM + CA1) in the year prior to AD conversion. Additionally, the local thickness-decreasing rate shows the highest difference of 2.89%/year between the pMCI and sMCI groups in the same region. These findings suggest distinct patterns of atrophy between the two groups, and the measurements that exhibit significant differences may serve as potential indicators for differentiating the two groups 1 year prior to AD conversion.

4.3 | Limitations and future work

Our study has two primary limitations. First, the hippocampal subfields are obtained through surface alignment of a probabilistic atlas derived from histology, rather than individual segmentation of subfields in each participant's hippocampus. Our method allows for direct comparison with histological research findings associated with the atlas, but it may not accurately represent the true subfield boundaries in each individual's hippocampus. Secondly, our statistical analysis method imposes strict inclusion criteria for the data, requiring three 3 T MRI T1-weighted scans with 1 year intermittent. As a result, our sample size is relatively small. Future directions for this research include incorporating subfield morphometric analysis on larger longitudinal samples to identify valuable imaging markers for early detection of Alzheimer's disease.

5 | CONCLUSION

In this study, we propose a multiscale skeletal representation (*m-s-rep*) to characterize the hippocampal shape from a small-to-large scale based on longitudinal 3T T1-weighted MR images. Based on this method, we investigate hippocampal atrophy patterns associated with the amyloid- β positive pMCI and sMCI. Quantification of local hippocampal atrophy by the proposed method discovers progressive local atrophy pattern that agree with consistent histological and 7 T MRI findings. The atrophy of hippocampus in early AD progression is dominated by a reduction in the lateral-medial width of the bilateral hippocampus, as well as rapid atrophy in the medial head region. Moreover, the differences between pMCI and sMCI extend from the body to the head of the hippocampus, indicating distinctive hippocampal atrophy trajectories between the pMCI and sMCI patients. In the 2 years

leading up to conversion, the right hippocampus demonstrates more severe and widespread atrophy in both the head and body regions, affecting areas such as CA1, SUB, and CA3. These findings highlight the effectiveness of our method in comprehensively assessing hippocampal atrophy using clinical data. Our approach offers a potential quantitative tool for evaluating hippocampal morphology, which can aid in the pre-diagnosis and prognosis of Alzheimer's disease.

AUTHOR CONTRIBUTIONS

Na Gao did data cleaning, processing, statistical analyses and drafted the manuscript and figures. Zhiyuan Liu assisted the data processing and drafted the manuscript. Yuesheng Deng and Hantao Chen collected and preprocessed the data. Chenfei Ye assisted the experiment design and refined the manuscript. Qi Yang supervised data processing. Ting Ma conceived and supervised the whole study, and revised the manuscript.

ACKNOWLEDGMENTS

The authors appreciate Professor Stephen M. Pizer (Department of Computer Science, University of North Carolina at Chapel Hill) and James Fishbaugh (Kitware, Inc.) for providing helpful advices for this study. The authors thank Ran Li for giving suggestions on plotting the figures. This study is supported by grants from the National Natural Science Foundation of P.R. China (62276081, 62106113), Innovation Team and Talents Cultivation Program of National Administration of Traditional Chinese Medicine (NO:ZYCYXTD-C-202004), Basic Research Foundation of Shenzhen Science and Technology Stable Support Program (GXWD20201230155427003-20200822115709001).

CONFLICT OF INTEREST STATEMENT

The authors declare no competing interests.

DATA AVAILABILITY STATEMENT

Data supporting the findings of this study were enrolled from Alzheimer's Disease Neuroimaging Initiative (ADNI) database: www.loni.ucla.edu/ADNI/. The inclusion and exclusion criteria were listed in "Datasets" section of manuscripts. The corresponding author has full access to the data and codes used in this study, which are available on reasonable request.

ORCID

Na Gao  <https://orcid.org/0000-0001-8516-9777>

Ting Ma  <https://orcid.org/0000-0001-8819-6228>

REFERENCES

- Adler, D. H., Wisse, L. E. M., Ittyerah, R., Pluta, J. B., Ding, S. L., Xie, L., Wang, J., Kadivar, S., Robinson, J. L., Schuck, T., Trojanowski, J. Q., Grossman, M., Detre, J. A., Elliott, M. A., Toledo, J. B., Liu, W., Pickup, S., Miller, M. I., Das, S. R., ... Yushkevich, P. A. (2018). Characterizing the human hippocampus in aging and Alzheimer's disease using a computational atlas derived from ex vivo MRI and histology. *Proceedings of the National Academy of Sciences of the United States of America*, 115, 4252–4257.

- Avants, B., Epstein, C., Grossman, M., & Gee, J. (2008). Symmetric diffeomorphic image registration with cross-correlation: Evaluating automated labeling of elderly and neurodegenerative brain. *Medical Image Analysis*, 12, 26–41.
- Benjamini, Y., & Yekutieli, D. (2001). The control of the false discovery rate in multiple testing under dependency. *The Annals of Statistics*, 29, 1165–1188.
- Biffi, C., Cerrolaza, J. J., Tarroni, G., Bai, W., de Marvao, A., Oktay, O., Ledig, C., le Folgoc, L., Kamnitsas, K., Doumou, G., Duan, J., Prasad, S. K., Cook, S. A., O'Regan, D. P., & Rueckert, D. (2020). Explainable anatomical shape analysis through deep hierarchical generative models. *IEEE Transactions on Medical Imaging*, 39, 2088–2099.
- Braak, E., & Braak, H. (1997a). Alzheimer's disease: Transiently developing dendritic changes in pyramidal cells of sector CA1 of the Ammon's horn. *Acta Neuropathologica*, 93, 323–325.
- Braak, H., & Braak, E. (1991). Neuropathological staging of Alzheimer-related changes. *Acta Neuropathologica*, 82, 239–259.
- Braak, H., & Braak, E. (1997b). Staging of Alzheimer-related cortical destruction. *International Psychogeriatrics*, 9(1), 257–261; discussion 269–272.
- Braak, H., Braak, E., & Bohl, J. (2004). Staging of Alzheimer-related cortical destruction. *European Neurology*, 33, 403–408.
- Chapleau, M., Bedetti, C., Devenyi, G. A., Sheldon, S., Rosen, H. J., Miller, B. L., Gorno-Tempini, M. L., Chakravarty, M. M., & Brambati, S. M. (2020). Deformation-based shape analysis of the hippocampus in the semantic variant of primary progressive aphasia and Alzheimer's disease. *NeuroImage: Clinical*, 27, 102305.
- Chauveau, L., Kuhn, E., Palix, C., Felisatti, F., Ourry, V., de la Sayette, V., Chételat, G., & de Flores, R. (2021). Medial temporal lobe subregional atrophy in aging and Alzheimer's disease: A longitudinal study. *Frontiers in Aging Neuroscience*, 13, 750154.
- Chincarini, A., Sensi, F., Rei, L., Gemme, G., Squarcia, S., Longo, R., Brun, F., Tangaro, S., Bellotti, R., Amoroso, N., Bocchetta, M., Redolfi, A., Bosco, P., Boccardi, M., Frisoni, G. B., Nobili, F., & Alzheimer's Disease Neuroimaging Initiative. (2016). Integrating longitudinal information in hippocampal volume measurements for the early detection of Alzheimer's disease. *NeuroImage*, 125, 834–847.
- Das, S. R., Avants, B. B., Pluta, J., Wang, H., Suh, J. W., Weiner, M. W., Mueller, S. G., & Yushkevich, P. A. (2012). Measuring longitudinal change in the hippocampal formation from in vivo high-resolution T2-weighted MRI. *NeuroImage*, 60, 1266–1279.
- de Flores, R., la Joie, R., & Chételat, G. (2015). Structural imaging of hippocampal subfields in healthy aging and Alzheimer's disease. *Neuroscience*, 309, 29–50.
- DeKraker, J., Köhler, S., & Khan, A. R. (2021). Surface-based hippocampal subfield segmentation. *Trends in Neurosciences*, 44, 856–863.
- Dubois, B., Feldman, H. H., Jacova, C., Hampel, H., Molinuevo, J. L., Blennow, K., DeKosky, S. T., Gauthier, S., Selkoe, D., Bateman, R., Cappa, S., Crutch, S., Engelborghs, S., Frisoni, G. B., Fox, N. C., Galasko, D., Habert, M. O., Jicha, G. A., Nordberg, A., ... Cummings, J. L. (2014). Advancing research diagnostic criteria for Alzheimer's disease: The IWG-2 criteria. *Lancet Neurology*, 13, 614–629.
- Fraser, M. A., Shaw, M. E., & Cherbuin, N. (2015). A systematic review and meta-analysis of longitudinal hippocampal atrophy in healthy human ageing. *NeuroImage*, 112, 364–374.
- Frisoni, G. B., Fox, N. C., Jack, C. R., Jr., Scheltens, P., & Thompson, P. M. (2010). The clinical use of structural MRI in Alzheimer disease. *Nature Reviews Neurology*, 6, 67–77.
- Fukutani, Y., Cairns, N. J., Shiozawa, M., Sasaki, K., Sudo, S., Isaki, K., & Lantos, P. L. (2000). Neuronal loss and neurofibrillary degeneration in the hippocampal cortex in late-onset sporadic Alzheimer's disease. *Psychiatry and Clinical Neurosciences*, 54, 523–529.
- Gabere, M., Thu Pham, N. T., Graff-Radford, J., Machulda, M. M., Duffy, J. R., Josephs, K. A., Whitwell, J. L., & for Alzheimer's Disease Neuroimaging Initiative. (2020). Automated hippocampal subfield volumetric analyses in atypical Alzheimer's disease. *Journal of Alzheimer's Disease*, 78, 927–937.
- Gerardin, E., Chételat, G., Chupin, M., Cuingnet, R., Desgranges, B., Kim, H. S., Niethammer, M., Dubois, B., Lehericy, S., Garnero, L., Eustache, F., Colliot, O., & Alzheimer's Disease Neuroimaging Initiative. (2009). Multidimensional classification of hippocampal shape features discriminates Alzheimer's disease and mild cognitive impairment from normal aging. *NeuroImage*, 47, 1476–1486.
- Greve, D. N., & Fischl, B. (2009). Accurate and robust brain image alignment using boundary-based registration. *NeuroImage*, 48, 63–72.
- Gunten, A., Kovari, E., Bussiere, T., Rivara, C., Gold, G., Bouras, C., Hof, P., & Giannakopoulos, P. (2006). Cognitive impact of neuronal pathology in the entorhinal cortex and CA1 field in Alzheimer's disease. *Neurobiology of Aging*, 27, 270–277.
- Hill, D. L. G., Schwarz, A. J., Isaac, M., Pani, L., Vamvakas, S., Hemmings, R., Carrillo, M. C., Yu, P., Sun, J., Beckett, L., Boccardi, M., Brewer, J., Brumfield, M., Cantillon, M., Cole, P. E., Fox, N., Frisoni, G. B., Jack, C., Kelleher, T., ... Stephenson, D. (2014). Coalition against major diseases/European medicines agency biomarker qualification of hippocampal volume for enrichment of clinical trials in predementia stages of Alzheimer's disease. *Alzheimer's Dement*, 10(4), 421–429.e3.
- Holland, D., McEvoy, L. K., Dale, A. M., & the Alzheimer's Disease Neuroimaging Initiative. (2012). Unbiased comparison of sample size estimates from longitudinal structural measures in ADNI. *Human Brain Mapping*, 33, 2586–2602.
- Iglesias, J. E., van Leemput, K., Augustinack, J., Insausti, R., Fischl, B., Reuter, M., & Alzheimer's Disease Neuroimaging Initiative. (2016). Bayesian longitudinal segmentation of hippocampal substructures in brain MRI using subject-specific atlases. *NeuroImage*, 141, 542–555.
- Jack, C. R., Petersen, R. C., Xu, Y., O'Brien, P. C., Smith, G. E., Ivnik, R. J., Boeve, B. F., Tangalos, E. G., & Kokmen, E. (2000). Rates of hippocampal atrophy correlate with change in clinical status in aging and AD. *Neurology*, 55, 484–490.
- Jenkinson, M., Bannister, P., Brady, M., & Smith, S. (2002). Improved optimization for the robust and accurate linear registration and motion correction of brain images. *NeuroImage*, 17, 825–841.
- Jones, S. E., Buchbinder, B. R., & Aharon, I. (2000). Three-dimensional mapping of cortical thickness using Laplace's equation. *Human Brain Mapping*, 11, 12–32.
- Kaushik, S., Vani, K., Chumber, S., Anand, K. S., & Dharmija, R. K. (2020). Evaluation of MR visual rating scales in major forms of dementia. *Journal of Neurosciences in Rural Practice*, 12, 16–23.
- Kerchner, G. A., Hess, C. P., Hammond-Rosenbluth, K. E., Xu, D., Rabinovici, G. D., Kelley, D. A. C., Vigneron, D. B., Nelson, S. J., & Miller, B. L. (2010). Hippocampal CA1 apical neuropil atrophy in mild Alzheimer disease visualized with 7-T MRI. *Neurology*, 75, 1381–1387.
- Kharabian Masouleh, S., Eickhoff, S. B., Zeighami, Y., Lewis, L. B., Dahnke, R., Gaser, C., Chouinard-Decorte, F., Lepage, C., Scholtens, L. H., Hoffstaedter, F., Glahn, D. C., Blangero, J., Evans, A. C., Genov, S., & Valk, S. L. (2020). Influence of processing pipeline on cortical thickness measurement. *Cerebral Cortex*, 30, 5014–5027.
- Kril, J. J., Patel, S., Harding, A. J., & Halliday, G. M. (2002). Patients with vascular dementia due to microvascular pathology have significant hippocampal neuronal loss. *Journal of Neurology Neurosurgery and Psychiatry*, 72, 747–751.
- Kulason, S., Tward, D. J., Brown, T., Sicut, C. S., Liu, C. F., Ratnanather, J. T., Younes, L., Bakker, A., Gallagher, M., Albert, M., Miller, M. I., & Alzheimer's Disease Neuroimaging Initiative. (2019). Cortical thickness atrophy in the transentorhinal cortex in mild cognitive impairment. *NeuroImage-Clinical*, 21, 101617.
- Lace, G., Savva, G. M., Forster, G., de Silva, R., Brayne, C., Matthews, F. E., Barclay, J. J., Dakin, L., Ince, P. G., Wharton, S. B., & MRC-CFAS. (2009). Hippocampal tau pathology is related to neuroanatomical connections: An ageing population-based study. *Brain*, 132, 1324–1334.

- Landau, S. M., Lu, M., Joshi, A. D., Pontecorvo, M., Mintun, M. A., Trojanowski, J. Q., Shaw, L. M., Jagust, W. J., & for the Alzheimer's Disease Neuroimaging Initiative. (2013). Comparing positron emission tomography imaging and cerebrospinal fluid measurements of beta-amyloid. *Annals of Neurology*, 74(6), 826–836.
- Ledig, C., Schuh, A., Guerrero, R., Heckemann, R. A., & Rueckert, D. (2018). Structural brain imaging in Alzheimer's disease and mild cognitive impairment: biomarker analysis and shared morphometry database. *Scientific Reports*, 8, 11258.
- Leung, K. K., Barnes, J., Ridgway, G. R., Bartlett, J. W., Clarkson, M. J., Macdonald, K., Schuff, N., Fox, N. C., Ourselin, S., & Alzheimer's Disease Neuroimaging Initiative. (2010). Automated cross-sectional and longitudinal hippocampal volume measurement in mild cognitive impairment and Alzheimer's disease. *NeuroImage*, 51, 1345–1359.
- Liu, Z., Hong, J., Vicory, J., Damon, J. N., & Pizer, S. M. (2021). Fitting unbranching skeletal structures to objects. *Medical Image Analysis*, 70, 102020.
- Lombardi, G., Crescioli, G., Cavedo, E., Lucenteforte, E., Casazza, G., Bellatorre, A. G., Lista, C., Costantino, G., Frisoni, G., Virgili, G., Filippini, G., & Cochrane Dementia and Cognitive Improvement Group. (2020). Structural magnetic resonance imaging for the early diagnosis of dementia due to Alzheimer's disease in people with mild cognitive impairment. *Cochrane Database of Systematic Reviews*, 3, CD009628.
- Martin, S. B., Smith, C. D., Collins, H. R., Schmitt, F. A., & Gold, B. T. (2010). Evidence that volume of anterior medial temporal lobe is reduced in seniors destined for mild cognitive impairment. *Neurobiology of Aging*, 31, 1099–1106.
- McKiernan, E. F., & O'Brien, J. T. (2017). 7T MRI for neurodegenerative dementias in vivo: A systematic review of the literature. *Journal of Neurology Neurosurgery and Psychiatry*, 88, 564–574.
- Moon, S. W., Lee, B., & Choi, Y. C. (2018). Changes in the hippocampal volume and shape in early-onset mild cognitive impairment. *Psychiatry Investigation*, 15, 531–537.
- Morra, J. H., Tu, Z., Apostolova, L. G., Green, A. E., Avedissian, C., Madsen, S. K., Parikshak, N., Toga, A. W., Clifford, J. R. Jr., Schuff, N., Weiner, M. W., Thompson, P. M., & Alzheimer's Disease Neuroimaging Initiative. (2009). Automated mapping of hippocampal atrophy in 1-year repeat MRI data from 490 subjects with Alzheimer's disease, mild cognitive impairment, and elderly controls. *NeuroImage*, 45, S3–S15.
- Padurariu, M., Ciobica, A., Mavroudis, I., Fotiou, D., & Baloyannis, S. (2012). Hippocampal neuronal loss in the Ca1 and Ca3 areas of Alzheimer's disease patients. *Psychiatra Danubina*, 24, 152–158.
- Pizer, S. M., Jung, S., Goswami, D., Vicory, J., Zhao, X., Chaudhuri, R., Damon, J. N., Huckemann, S., & Marron, J. S. (2013). Nested sphere statistics of skeletal models. In M. Breuß, A. Bruckstein, & P. Maragos (Eds.), *Innovations for Shape Analysis: Models and Algorithms*. Springer Berlin Heidelberg.
- Pizer, S. M., Hong, J., Vicory, J., Liu, Z., Marron, J. S., Choi, H. Y., Damon, J., Jung, S., Paniagua, B., Schulz, J., Sharma, A., Tu, L., & Wang, J. (2020). Object shape representation via skeletal models (s-reps) and statistical analysis. In *Riemannian geometric statistics in medical image analysis* (pp. 233–271). Elsevier.
- Pizer, S. M., Marron, J. S., Damon, J. N., Vicory, J., Krishna, A., Liu, Z., & Taheri, M. (2022). Skeletons, object shape, statistics. *Frontiers in computer science*, 4, 842637.
- Renka, R. J. (2005). Shape-preserving interpolation by fair discrete G(3) space curves. *Computer Aided Geometric Design*, 22, 793–809.
- Ruchinkas, R., Nguyen, T., Womack, K., Khera, A., Yu, F. F., & Kelley, B. J. (2022). Diagnostic utility of hippocampal volumetric data in a memory disorder clinic setting. *Cognitive and Behavioral Neurology*, 35, 66–75.
- Scheff, S. W., Price, D. A., DeKosky, S. T., Mufson, E. J., & Mufson, E. J. (2007). Synaptic alterations in CA1 in mild Alzheimer disease and mild cognitive impairment. *Neurology*, 68, 1501–1508.
- Schönheit, B., Zarski, R., & Ohm, T. G. (2004). Spatial and temporal relationships between plaques and tangles in Alzheimer-pathology. *Neurobiology of Aging*, 25, 697–711.
- Schuff, N., Woerner, N., Boreta, L., Kornfield, T., Shaw, L. M., Trojanowski, J. Q., Thompson, P. M., Clifford, J. R. Jr., Weiner, M. W., & Alzheimer's Disease Neuroimaging Initiative. (2009). MRI of hippocampal volume loss in early Alzheimer's disease in relation to ApoE genotype and biomarkers. *Brain*, 132, 1067–1077.
- Schulz, J., Pizer, S. M., Marron, J. S., & Godtliebsen, F. (2016). Non-linear hypothesis testing of geometric object properties of shapes applied to hippocampi. *Journal of Mathematical Imaging and Vision*, 54, 15–34.
- Shaw, L. M., Vanderstichele, H., Knapik-Czajka, M., Clark, C. M., Aisen, P. S., Petersen, R. C., Blennow, K., Soares, H., Simon, A., Lewczuk, P., Dean, R., Siemers, E., Potter, W., Lee, V. M. Y., Trojanowski, J. Q., & Alzheimer's Disease Neuroimaging Initiative. (2009). Cerebrospinal fluid biomarker signature in Alzheimer's disease neuroimaging initiative subjects. *Annals of Neurology*, 65(4), 403–413.
- Shi, J., Thompson, P. M., Gutman, B., Wang, Y., & Alzheimer's Disease Neuroimaging Initiative. (2013). Surface fluid registration of conformal representation: Application to detect disease burden and genetic influence on hippocampus. *NeuroImage*, 78, 111–134.
- Styner, M., Oguz, I., Xu, S., Brechbühler, C., Pantazis, D., Levitt, J. J., Shenton, M. E., & Gerig, G. (2006). Framework for the statistical shape analysis of brain structures using SPHARM-PDM. *Insight Journal*, 1071, 242–250.
- Tang, X. Y., Holland, D., Dale, A. M., Younes, L., Miller, M. I., & for the Alzheimer's Disease Neuroimaging Initiative. (2015). The Diffeomorphometry of regional shape change rates and its relevance to cognitive deterioration in mild cognitive impairment and Alzheimer's disease. *Human Brain Mapping*, 36, 2093–2117.
- Tu, L. Y., Styner, M., Vicory, J., Elhabian, S., Wang, R., Hong, J., Paniagua, B., Prieto, J. C., Yang, D., Whitaker, R., & Pizer, S. M. (2018). Skeletal shape correspondence through entropy. *IEEE Transactions on Medical Imaging*, 37, 1–11.
- Tustison, N. J., Cook, P. A., Klein, A., Song, G., das, S. R., Duda, J. T., Kandel, B. M., van Strien, N., Stone, J. R., Gee, J. C., & Avants, B. B. (2014). Large-scale evaluation of ANTs and FreeSurfer cortical thickness measurements. *NeuroImage*, 99, 166–179.
- Tward, D. J., Sicut, C. S., Brown, T., Bakker, A., Gallagher, M., Albert, M., Miller, M., & Alzheimer's Disease Neuroimaging Initiative. (2017). Entorhinal and transentorhinal atrophy in mild cognitive impairment using longitudinal diffeomorphometry. *Alzheimers Dement (Amst)*, 9, 41–50.
- van Oostveen, W. M., & de Lange, E. C. M. (2021). Imaging techniques in Alzheimer's disease: A review of applications in early diagnosis and longitudinal monitoring. *International Journal of Molecular Sciences*, 22, 2110–2143.
- Witter, M. P., Amaral, D. G., 2004. *Hippocampal formation*. Orlando, FL: Academic Press.
- Wolz, R., Heckemann, R. A., Aljabar, P., Hajnal, J. V., Hammers, A., Lötjönen, J., Rueckert, D., & Alzheimer's Disease Neuroimaging Initiative. (2010). Measurement of hippocampal atrophy using 4D graph-cut segmentation: Application to ADNI. *NeuroImage*, 52, 109–118.
- Xie, L., Wisse, L. E. M., das, S. R., Vergnet, N., Dong, M., Ittyerah, R., Flores, R., Yushkevich, P. A., Wolk, D. A., & for the Alzheimer's Disease Neuroimaging Initiative. (2020). Longitudinal atrophy in early Braak regions in preclinical Alzheimer's disease. *Human Brain Mapping*, 41, 4704–4717.
- Zeng, D. B., Li, Q. L., Ma, B., & Li, S. (2020). Hippocampus segmentation for preterm and aging brains using 3D densely connected fully convolutional networks. *IEEE Access*, 8, 97032–97044.

- Zeng, Q., Li, K., Luo, X., Wang, S., Xu, X., Li, Z., Zhang, T., Liu, X., Fu, Y., Xu, X., Wang, C., Wang, T., Zhou, J., Liu, Z., Chen, Y., Huang, P., Zhang, M., & for the Alzheimer's Disease Neuroimaging Initiative. (2021). Distinct atrophy pattern of hippocampal subfields in patients with progressive and stable mild cognitive impairment: A longitudinal MRI study. *Journal of Alzheimers Disease*, 79, 237–247.
- Zhang, L., Mak, E., Reilhac, A., Shim, H. Y., Ng, K. K., Ong, M. Q. W., Ji, F., Chong, E. J. Y., Xu, X., Wong, Z. X., Stephenson, M. C., Venkatasubramanian, N., Tan, B. Y., O'Brien, J. T., Zhou, J. H., Chen, C. L. H., & the Alzheimer's Disease Neuroimaging Initiative. (2020). Longitudinal trajectory of amyloid-related hippocampal subfield atrophy in nondemented elderly. *Human Brain Mapping*, 41, 2037–2047.

SUPPORTING INFORMATION

Additional supporting information can be found online in the Supporting Information section at the end of this article.

How to cite this article: Gao, N., Liu, Z., Deng, Y., Chen, H., Ye, C., Yang, Q., & Ma, T. (2023). MR-based spatiotemporal anisotropic atrophy evaluation of hippocampus in Alzheimer's disease progression by multiscale skeletal representation. *Human Brain Mapping*, 44(15), 5180–5197. <https://doi.org/10.1002/hbm.26460>